EUROPEAN ORGANIZATION FOR NUCLEAR RESEARCH

CERN-EP-2017-216
21 Aug 2017

π^0 and η meson production in proton-proton collisions at $\sqrt{s} = 8$ TeV

ALICE Collaboration*

Abstract

An invariant differential cross section measurement of inclusive π^0 and η meson production at mid-rapidity in pp collisions at $\sqrt{s} = 8$ TeV was carried out by the ALICE experiment at the LHC. The spectra of neutral mesons π^0 and η were measured in transverse momentum ranges of $0.3 < p_{\mathrm{T}} < 35$ GeV/c and $0.5 < p_{\mathrm{T}} < 35$ GeV/c, respectively. Next-to-leading order perturbative QCD calculations using fragmentation functions DSS14 for π^0 and AESSS for η overestimate the cross sections of both neutral mesons, but agree with the measured η/π^0 ratio within uncertainties. The results are also compared with PYTHIA 8.2 predictions for which the Monash 2013 tune yields the best agreement with the measured neutral meson spectra. The measurements confirm a universal behavior of the η/π^0 ratio seen for NA27, PHENIX and ALICE data for pp collisions from $\sqrt{s} = 27.5$ GeV to $\sqrt{s} = 8$ TeV within experimental uncertainties. A relation between the π^0 and η production cross sections for pp collisions at $\sqrt{s} = 8$ TeV is given by m_{T} scaling for $p_{\mathrm{T}} > 3.5$ GeV/c. However, a deviation from this empirical scaling law is observed for transverse momenta below $p_{\mathrm{T}} < 3.5$ GeV/c in the η/π^0 ratio with a significance of 6.2σ.

*See Appendix A for the list of collaboration members

1 Introduction

Measuring identified particle production in proton-proton (pp) collisions over wide kinematic ranges is considered an informative probe of strong interactions at high energies. Quantum Chromodynamics (QCD) is the fundamental theory of the strong interaction [1]. It succeeds in providing a qualitative description of a wide range of phenomena in hadronic collisions. At typical hadron collider energies its perturbative expansion (pQCD) permits a detailed quantitative comparison with experimental data. However, it remains a challenge to provide a consistent description of hadron spectra at all collision energies reached experimentally. In theoretical models, particle production is usually divided into two categories: the "soft" scattering regime describing particle production involving small momentum transfers and the "hard" scattering regime, responsible for producing particles with momenta of several GeV/c or more.

Only "hard" scattering processes with a sufficiently large transverse momentum transfer, Q^2, can be calculated using methods based on pQCD. High-momentum particles originate from the fragmentation of partons produced in scattering processes with large momentum transfer Q^2. The theoretical description of a "hard" scattering process can be factorized into parton distribution functions (PDF), the QCD matrix element and fragmentation functions (FF). PDFs describe the fraction of the proton's longitudinal momentum carried by a scattered parton, x, and FFs describe the ratio of the observed hadron momentum to the final-state parton momentum, z, respectively. Comprehensive parametrizations of PDFs and FFs are derived from global fits to the experimental data at various collision energies. The energies reached at the LHC [2] open up the domains in x and z not accessible at lower energy. In the past, experiments at the LHC consequently found discrepancies between the measured π^0 and η meson spectra [3–5] and pQCD calculations based on fragmentation functions, which include mostly data from experiments below the TeV scale [6]. Since the gluon contribution becomes more dominant with increased center of mass energy, $\sqrt{s}$, [7], π^0 and η meson spectra at LHC energies provide new constraints on the gluon fragmentation via processes like $pp \to hX$. Recent progress in comprehensive global QCD analysis of parton-to-pion fragmentation functions at next-to-leading order (NLO) [8] derived from inclusive pion production in semi-inclusive electron-positron annihilation, deep-inelastic scattering and pp collisions over a wide energy range, including the LHC results [3], achieved a good and consistent description of pion spectra, including the latest measurements of π^0 and η spectra in pp collisions at $\sqrt{s} = 2.76$ TeV [9] and 7 TeV [3]. One of the conclusions of that analysis was the reduced meson production from gluon fragmentation, which turns out to be at tension with previously available data obtained at RHIC [10]. In the quark model, the π^0 consists of light-flavor quark-antiquark pairs $u\bar{u}$ and $d\bar{d}$, whereas the η additionally contains hidden strangeness $s\bar{s}$. Measurements of both neutral mesons are thus of particular interest due to their different quark content as they help to constrain the PDFs and FFs of the s quark.

The majority of particles at low $p_{\rm T}$ are produced in "soft" processes involving a small momentum transfer, Q^2. In this regime, the pQCD calculations are not applicable for description of the production mechanisms and phenomenological models are based on previous measurements of neutral meson production cross sections or other light mesons by other experiments at lower collision energies. Particle production measurements at transverse momenta down to a few hundred MeV/c, as reported here, are particularly important to further constrain such models.

The importance of precise identified particle production measurements is underlined by various empirical rules observed in relative particle yields which allow estimates of the hadronic background of rare probes such as direct photons, dileptons and heavy-quark production. Almost all lower-energy experiments from ISR to RHIC reported the observation of $m_{\rm T}$ scaling in particle production over wide $p_{\rm T}$ ranges [11]. The practical use of $m_{\rm T}$ scaling is the ability to derive the $p_{\rm T}$-dependent differential yields of most of particles from the well measured light-flavor mesons, like pions and kaons, by assuming that the meson spectra can be described as a function of transverse mass $m_{\rm T}$: $E{\rm d}^3\sigma/{\rm d}p^3 = C^{\rm m} f(m_{\rm T})$, where the function $f(m_{\rm T})$ is universal for all hadron species, so that their spectra share the same shape up to a normalization factor $C^{\rm m}$. However, phenomenological analyses of new data delivered by the LHC experiments [12] indicate that m_{T} scaling might be violated at higher p_{T} compared to lower collision energies. Therefore, precise measurements of identified hadron spectra over wide transverse momentum ranges at different LHC energies are of particular importance for the quantitative description of particle production at the LHC.

In this paper, the differential invariant production cross sections, $E\mathrm{d}^3\sigma/\mathrm{d}p^3$, of π^0 and η mesons and the particle production ratio η/π^0 are presented. These have been measured over wide p_{T} ranges at mid-rapidity in pp collisions at $\sqrt{s} =$ 8 TeV by ALICE. The new experimental results are compared with pQCD calculations using PDF MSTW08 [13] with FF DSS14 [8] for π^0 and accordingly CTEQ6M5 [14] with AESSS [15] for η, as well as the PYTHIA8.210 Monte Carlo (MC) event generator [16] with the tunes 4C [17] and Monash 2013 [18].

This paper is organized as follows: In Sec. 2, the ALICE experiment is briefly described with the focus on the detectors used in this analysis, namely the calorimeters and the central tracking systems. Sec. 3 describes the datasets, the event selection and also introduces the calorimeter triggers used in this analysis. In Sec. 4, the reconstruction principles for neutral mesons are introduced. Furthermore, the determination of correction factors, which are used to calculate the differential invariant cross sections from the measured raw yields, is described. Sec. 5 discusses the various contributions to the statistical and systematic uncertainties of the measurements. In Sec. 6, the p_{T} differential invariant cross sections for π^0 and η meson production in pp collisions at $\sqrt{s} =$ 8 TeV are presented and compared with pQCD calculations. Subsequently, the measured ratio of η/π^0 is presented and compared to the same theoretical models. Sec. 7 concludes the paper with a summary of the obtained results.

2 Detector description

Neutral mesons, π^0 and η, were reconstructed via their two-photon decay channels. In the present analysis, two fundamentally different detection methods were used to reconstruct decay photons. The first method exploits the measurement of photons using electromagnetic calorimeters. Two such calorimeters are available in ALICE [19, 20]: the Electromagnetic Calorimeter (EMCal) [21] and the Photon Spectrometer (PHOS) [22]. The second method of photon detection makes use of photons converted into e^+e^- pairs within the inner detector material located between the interaction point and a radius which corresponds to the midpoint between the inner and outer field cage of the Time Projection Chamber (TPC). These electron-positron pairs, originating at secondary vertices (V^0), are reconstructed by the main tracking systems in ALICE centered at mid-rapidity and consisting of the Inner Tracking System (ITS) [23] and the TPC [24]. The aforementioned detectors are described below, noting the detector configurations during pp data taking at $\sqrt{s} =$ 8 TeV in 2012.

The EMCal detector [21] is a sampling electromagnetic calorimeter. Its active elements, or cells, are composed of 77 alternating layers of lead and plastic scintillator providing a radiation length of $20.1\,X_0$. The scintillation light in each layer is collected by wavelength shifting fibers perpendicular to the face of each cell. The fibers are connected to 5×5 mm^2 active area Avalanche Photo Diodes (APDs) to detect the generated scintillation light. Each cell has a size of $\Delta\eta \times \Delta\phi = 0.0143 \times 0.0143$ ($\approx 6.0 \times 6.0$ cm^2), corresponding to approximately twice the Molière radius. Groups of 2×2 cells are combined into modules, which are further combined into arrays of 12×24 modules called supermodules. In total, there were ten active, full EMCal supermodules, covering $\Delta\phi = 100^\circ$ in azimuth and $|\eta| < 0.7$ in pseudorapidity with a total number of 11,520 cells. The EMCal is located at a radial distance of 4.28 m at the closest point from the nominal collision vertex. The intrinsic energy resolution of the EMCal is parametrized as $\sigma_E/E = 4.8\%/E \oplus 11.3\%/\sqrt{E} \oplus 1.7\%$ with energy E in units of GeV [25]. The relative energy calibration of the detector has been performed by measuring, in each cell, the reconstructed π^0 mass in the invariant mass distribution of photon pairs built with one photon in the given cell. The achieved calibration level is estimated to be 3% and adds up quadratically to the constant term of the energy resolution.

The PHOS [19, 22] is a homogeneous electromagnetic calorimeter composed of lead tungstate, $PbWO_4$. The size of its elementary active units, also called cells, is $\Delta\eta \times \Delta\phi = 0.004 \times 0.004$ ($\approx 2.2 \times 2.2$ cm^2). Thus, the lateral dimensions of the cells are slightly larger than the $PbWO_4$ Molière radius of 2 cm. APDs with an active area of 5×5 mm^2 detect the scintillation light generated within the detector cells. The spectrometer covers $\Delta\phi = 60°$ in azimuth and $|\eta| < 0.12$ in pseudorapidity and is located at a distance of 4.6 m from the interaction point. It is operated at a temperature of -25°C, at which the light yield of $PbWO_4$ increases by about a factor of three compared to room temperature. The energy resolution of the PHOS is $\sigma_E/E = 1.8\%/E \oplus 3.3\%/\sqrt{E} \oplus 1.1\%$, with E in units of GeV. The fine granularity of the detector enables the measurement of neutral pion candidates up to $p_{\mathrm{T}} \approx 50$ GeV/c.

The ITS [23] consists of three sub-detectors each with two layers to measure the trajectories of charged particles and to reconstruct primary vertices. The two innermost layers are the Silicon Pixel Detectors (SPD) positioned at radial distances of 3.9 cm and 7.6 cm. The middle two layers are Silicon Drift Detectors (SDD) located at 15.0 cm and 23.9 cm relative to the beam line. The outer two layers are Silicon Strip Detectors (SSD) located at radial distances of 38 cm and 43 cm. The two layers of SPD cover pseudorapidity ranges of $|\eta| < 2$ and $|\eta| < 1.4$, respectively. The SDD and SSD cover $|\eta| < 0.9$ and $|\eta| < 1.0$, accordingly.

The TPC [24] is a large (90 m^3) cylindrical drift detector filled with a gas mixture of Ne-CO_2-N_2 (85.7-9.5-4.8%). It covers a pseudorapidity range of $|\eta| < 0.9$ over full azimuth, providing up to 159 reconstructed space points per track. A magnetic field of $B = 0.5$ T is generated by a large solenoidal magnet surrounding the central barrel detectors. Charged tracks originating from the primary vertex can be reconstructed down to $p_{\mathrm{T}} \approx 100$ MeV/c and charged secondaries down to $p_{\mathrm{T}} \approx 50$ MeV/c [20]. The TPC provides particle identification via the measurement of energy loss dE/dx with a resolution of $\approx 5\%$ [24]. Beyond the outer radius of the TPC, the Transition Radiation Detector (TRD) and the Time-Of-Flight detector (TOF) provide additional particle identification information, as well as allowing for improved momentum resolution and added triggering capability. The detectors represent most of the material between the TPC and the EMCal and hence dominate the material budget uncertainty in the analysis. These detectors are missing in front of PHOS in order to provide a minimal radiation length to profit from the high resolution of the spectrometer.

The V0 detector is made up of two scintillator arrays (V0A and V0C) [26] covering $2.8 < \eta < 5.1$ and $-3.7 < \eta < -1.7$. It is used to provide a minimum bias trigger [27] and reduce background events [20]. It is also involved in the definition of calorimeter triggers [28, 29] and is used for luminosity determination as described in the next section.

In addition, the T0 detector [30] was used for luminosity determination. It consists of two arrays of Cherenkov counters, T0A and T0C, which respectively cover $4.61 < \eta < 4.92$ and $-3.28 < \eta < -2.97$. The T0 furthermore provides a precise timing signal to other detectors with a resolution of better than 50 ps, used as starting signal for the TOF detector for example.

3 Datasets and event selection

During the data taking period of pp collisions at $\sqrt{s} =$ 8 TeV in 2012, the LHC operated at high beam intensities of approximately 2×10^{14} protons per beam. Collisions at the ALICE interaction point were realised using a main-satellite bunch scheme, which involved collisions between high intensity main bunches and low intensity satellite bunches. The interaction probability per bunch-satellite crossing was about 0.01, corresponding to an average instantaneous luminosity of about 5×10^{30} cm^{-2}s^{-1}. Background events caused by beam-gas interactions or detector noise were rejected for analysis using the V0A and V0C timing information [20]. Pileup events, with more than one pp collision per bunch crossing, were rejected based on SPD pileup identification algorithms looking for multiple primary vertices in a single event [20]. Additionally, the SPD was used to reject background events by comparing the number of clusters to the multiplicity of tracklets found in the respective collision. Only events with a z-vertex position of $|z| < 10$ cm in the global ALICE coordinate system were accepted for analyses.

The reported analyses used events which were selected by two types of triggers: the ALICE minimum bias interaction trigger [27] and the calorimeter triggers, provided by the EMCal [28] and the PHOS [29], to enhance statistics at high p_{T} by selectively recording events with high energy deposits. The minimum bias trigger used is a level-0 (L0) trigger generated 1.2 μs after the interaction. It requires at least one hit in each V0A and V0C [26]. Both calorimeters also generate L0 triggers of the same latency as the minimum bias trigger. They are required to be in coincidence with the minimum bias trigger and select events with a deposited energy exceeding a nominal threshold in 4×4 adjacent cells in the respective calorimeter. The energy sum is formed by the sliding window algorithm which is used by the trigger region units (TRU). The summands are limited to one TRU, covering 8×48 cells in EMCal and 16×14 cells in PHOS. The L0 trigger is generated by EMCal or PHOS if at least one TRU of the respective calorimeter detects an energy sum above the threshold. These thresholds for the EMC- and PHOS-L0 triggers were set to $\overline{E}_{\text{EMC-L0}} \approx 2$ GeV and $\overline{E}_{\text{PHOS-L0}} \approx 4$ GeV, respectively. A level-1 (L1) photon trigger was also deployed for EMCal which inspects events preselected by the EMC-L0 trigger and generates a trigger signal within 6.2 μs after the interaction. This EMC-L1 trigger algorithm is similar to EMC-L0, but the sliding window algorithm inspects the whole supermodule instead of a single TRU, thus increasing the effective area by about one third. Moreover, a higher trigger threshold of $\overline{E}_{\text{EMC-L1}} \approx 8.4$ GeV was set to further improve the transverse momentum reach of EMCal measurements.

In order to correctly normalize each trigger, the rejection factors (RF) were determined by constructing the ratio of cluster energy spectra from minimum bias and triggered events. To further reduce the statistical uncertainties, the factor was always determined with respect to next lower threshold trigger. The cluster energy ratios have a steep turn-on near the respective trigger threshold energies. They reach constant plateaus at high energies where $RF_{\text{EMC-L0}} = 67.0 \pm 1.1$, $RF_{\text{PHOS-L0}} = (12.4 \pm 1.5) \times 10^3$ and $RF_{\text{EMC-L1}} = (14.9 \pm 0.3) \times 10^3$. The last factor was obtained by multiplying the two given rejection factors of the two EMCal triggers, see Fig. 1, as the RF for EMC-L1 to minimum bias trigger is of interest. Fig. 1 shows a plot of the trigger ratios used to determine the trigger rejection factors. The legend in

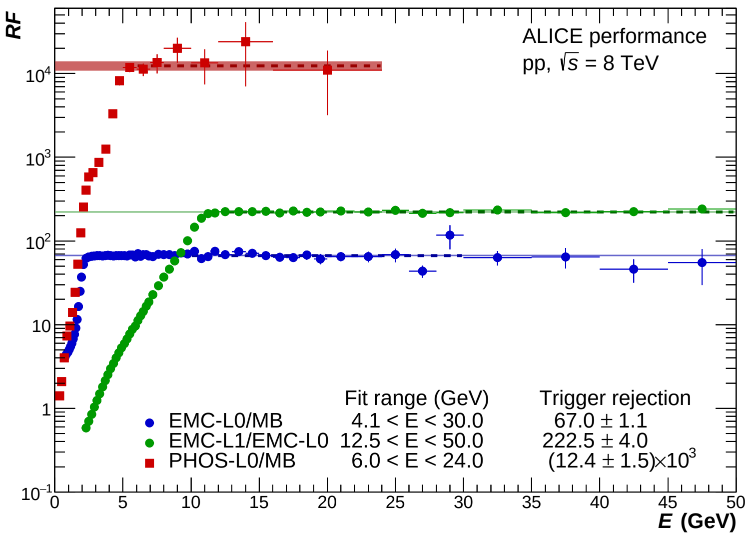

Fig. 1: Determination of trigger rejection factors for the used PHOS-L0 and EMC-L0/L1 triggers. The raw spectra of photon candidates for each trigger combination given in the legend are used to obtain the respective ratio of yields. The obtained distributions are then fitted with a constant in the illustrated energy ranges, yielding the quoted RFs. The uncertainties of RF determination are indicated in light colored uncertainty bands.

Fig. 1 indicates the fit ranges used to find the plateau values, illustrated by the dashed lines. Only the plateau regions of the RFs are of importance for the reported analyses. However, since EMC-L0 trigger becomes fully efficient only above its triggering threshold of $\overline{E}_{\text{EMC-L0}} \approx 2$ GeV, there is a change of slope visible in the turn-on region of the EMC-L1 trigger. The turn-on curve of the PHOS-L0 trigger also changes its slope due to a non-uniformity of the channels hardware gains.

The luminosity determination is based on the cross-section of the minimum bias trigger condition, $\sigma_{\text{MB}_\text{AND}}$, measured in a van der Meer (vdM) scan [31, 32]. The stability of the measured cross section throughout the whole data taking period was assessed by comparing the V0-based luminosity measurement with an independent luminosity signal, issued by the T0 detector. As discussed in [32], this comparison results in an overall normalization uncertainty of 2.6%, which includes contributions from both the vdM-based measurement and its stability over time. The integrated luminosity of each triggered sample was calculated with the number of analyzed events, N_{events}, the respective rejection factors, RF, and the minimum bias cross section, $\sigma_{\text{MB}_\text{AND}} = 55.80 \pm 1.45_{(\text{stat+sys})}$ mb [32], given by:

$$\mathscr{L}_{\text{int}} = \frac{N_{\text{events}}}{\sigma_{\text{MB}_\text{AND}}} \times RF \tag{1}$$

for which $RF = 1$ holds for the minimum bias trigger. As the good run lists for each detection method do not coincide, integrated luminosities are individually quoted for all cases in Tab. 1.

	$\mathscr{L}_{\text{int}}$ (nb^{-1})		
Reconstruction method	EMC & PCM-EMC	PHOS	PCM
MB trigger	$1.94 \pm 0.05_{\text{norm}}$	$1.25 \pm 0.04_{\text{norm}}$	$2.17 \pm 0.06_{\text{norm}}$
EMC-/PHOS-L0 trigger	$40.9 \pm 0.7_{\text{sys}} \pm 1.1_{\text{norm}}$	$135.6 \pm 16.8_{\text{sys}} \pm 3.6_{\text{norm}}$	-
EMC-L1 trigger	$615.0 \pm 15.0_{\text{sys}} \pm 16.0_{\text{norm}}$	-	-

Table 1: The analyzed luminosities considering the individual statistics for the different reconstruction methods and triggers. The neutral meson analyses using EMCal and hybrid PCM-EMCal used the same list of good runs as indicated by the combined column. The uncertainties denoted with "sys" reflect the systematical uncertainty of rejection factor determination, whereas "norm" represents the uncertainties entering from the cross section determination of minimum bias trigger [32].

4 Neutral meson reconstruction

Neutral mesons were reconstructed using the two electromagnetic calorimeters, EMCal and PHOS, a photon conversion method (PCM) and a hybrid method, PCM-EMCal, which combines one photon candidate from PCM and one from the EMCal, resulting in four different methods for π^0 and three for η mesons. It was not possible to measure η mesons using PHOS, due to the detector's limited acceptance and the wider opening angle of the photons from η decays. Both π^0 and η mesons were reconstructed via their two-photon decay channels with branching ratios of $98.823 \pm 0.034\%$ and $39.31 \pm 0.20\%$ [33] by means of invariant mass analyses. The hybrid PCM-EMCal measurement benefits from the high momentum resolution of the PCM, a high reconstruction efficiency and, crucially, the triggering capabilities of EMCal. Moreover, an extended p_{T} coverage was achieved compared to the standalone EMCal measurement, as there is no limitation due to cluster merging effects, discussed later in this section.

Photons and electrons/positrons generate electromagnetic showers when they enter an electromagnetic calorimeter. They usually spread their energy over multiple adjacent calorimeter cells. In order to reconstruct the full energy of particles, those adjacent cells are grouped into clusters, which is realized by a clusterization algorithm. The algorithm starts with highest energy cell in the recorded event whose energy exceeded E_{seed}. After finding the seed cell, adjacent cells with energy above E_{min} are added to the cluster. For the EMCal, the clusterization algorithm adds cells to the cluster as long as its energy is smaller than the previous one and stops the aggregation, if the adjacent cell has a higher energy than the current one. Clustering continues in the same way with the remaining cells until all cells are grouped into clusters. Cluster energies are then calculated by $E = \sum_i^{N_{\rm cell}} e_i$ where e_i stands for the energy recorded by the indicated cell. The values of $E_{\rm seed}$ and $E_{\rm min}$ depend on the energy resolution and the noise level of the front-end electronics. For the EMCal, values of $E_{\rm seed} = 500$ MeV and $E_{\rm min} = 100$ MeV were chosen. For the PHOS, these parameters were set to $E_{\rm seed} = 200$ MeV and $E_{\rm min} = 15$ MeV. Large clusters due to overlapping photon showers in the PHOS were separated into individual clusters by an unfolding method based on the knowledge of the lateral shape of the electromagnetic shower [34].

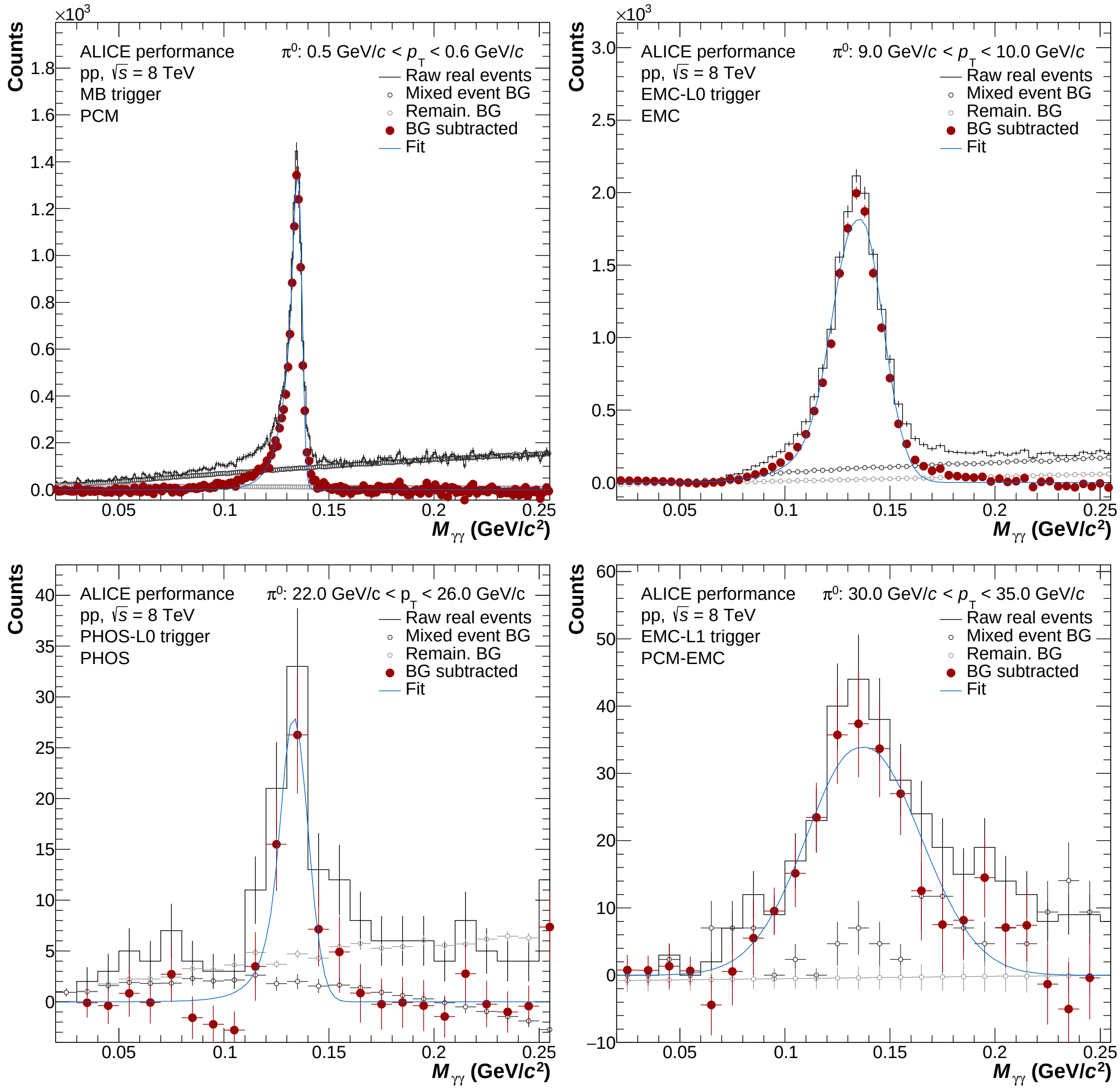

Fig. 2: Example invariant mass spectra in selected $p_{\rm T}$ slices for PCM (top left), PHOS (top right), EMC (bottom left) and PCM-EMC (bottom right) in the π^0 mass region. The black histograms show invariant mass distributions before any background subtraction. The grey points show mixed event and residual correlated background contributions, which have been subtracted from raw real events to obtain the signal displayed with red data points. The blue curves represent fits to the background subtracted invariant mass spectra.

Cell energies were calibrated for both calorimeters to provide best estimates for the cluster energies. After the cell-by-cell energy calibration of the EMCal [21, 25], an improved correction for the relative energy scale as well as for the residual misalignment of the EMCal between data and MC simulations was derived by making use of the good momentum resolution of the PCM photon in the hybrid PCM-EMCal method. Using this method, the neutral pion mass was evaluated as a function of EMCal cluster energy for data and MC in order to deduce a cluster energy correction for the simulation, for which the reconstructed neutral pion masses were adjusted to the measured mass positions in data. For $p_{\rm T} > 1$ GeV$/c$, the corrections are throughout of the order of 4%. Thus, a precise energy calibration scheme for the relevant energy regions was available for the reported analyses. It was found to be consistent for EMCal and hybrid PCM-EMCal analyses for π^0 as well as η mesons at the same time, hence demonstrating the validity of the procedure. The obtained mass position ratios from data and MC were computed for all transverse momentum bins and were fitted with a constant. Residual offsets of 0.005$\pm$0.043% and 0.14$\pm$0.13% were found for π^0 and η mesons for the EMCal analysis, whereas 0.001$\pm$0.042% and 0.02$\pm$0.14% were obtained for PCM-EMCal. For the PHOS, the energy deposition in each cell was calibrated by adjusting the π^0 peak position in the invariant mass spectra of photon pairs to the true mass of the π^0 meson. The accuracy of this calibration procedure was estimated to be better than 1%. It was evaluated from a comparison of the π^0 peak width in calibrated data and MC simulations by introducing random, normal-distributed decalibration parameters to the MC simulation.

Photon identification criteria were applied to the sample of reconstructed clusters in order to primarily select true photon candidates. For the photon reconstruction with PHOS, relatively loose identification cuts were applied to the reconstructed clusters because the shower overlap is negligible and the combinatorial background was found to be small in pp collisions. A minimum cluster energy $E_{\rm cluster} > 0.3$ GeV as well as a minimum number of cells forming a cluster, $N_{\rm cell} \geq 3$, were required in order to reject minimum ionizing charged particles. For the EMCal, a minimum energy cut of $E_{\rm cluster} > 0.7$ GeV was applied and the minimum number of cells grouped in a cluster was set to $N_{\rm cell} \geq 2$. Furthermore, the selection criteria of $|\eta| < 0.67$ and 1.40 rad $< \varphi <$ 3.15 rad were imposed for EMCal clusters. Pileup from multiple events which may occur within a readout interval of the front-end electronics was rejected by applying a cluster timing cut relative to the collision time of $-25 < t_{\rm cluster} < 25$ ns for the PHOS and $-35 < t_{\rm cluster} < 25$ ns for the EMCal. Thus, photon candidates from different bunch crossings were removed with a high efficiency of >99%. For the EMCal, all clusters matched with a primary charged track were rejected. This track matching procedure, referred to as general track matching below, used a track momentum-dependent matching in η and φ, beginning from $|\Delta\eta| < 0.04$ and $|\Delta\varphi| < 0.09$ for very low track momenta of $p_{\rm T} < 0.5$ GeV$/c$ and going down to $|\Delta\eta| < 0.01$ and $|\Delta\varphi| < 0.015$ for highest track momenta, using the $p_{\rm T}$ dependent matching conditions $|\Delta\eta| < 0.01 + (p_{\rm T} + 4.07)^{-2.5}$ and $|\Delta\varphi| < 0.015 + (p_{\rm T} + 3.65)^{-2}$. Applying those conditions, a primary track to cluster matching efficiency of more than 95% was obtained over the full transverse momentum range, rising above 98% for the analyzed EMCal triggered datasets for momenta beyond 10 GeV$/c$. To further enhance the photon purity and to reject neutral hadrons, a cluster shape cut of $0.1 \leq \sigma^2_{\rm long} \leq 0.7$ was applied for EMCal clusters, where $\sigma^2_{\rm long}$ stands for the smaller eigenvalue of the dispersion matrix of the shower shape ellipse defined by the responding cells and their energy contributions to the cluster [9, 35]. The lower threshold of $\sigma^2_{\rm long}$ was chosen to remove contamination caused by neutrons hitting the APDs of the readout electronics.

Photons convert within the detector material of ALICE with a probability of about 8.5%. The reconstruction of such photon conversion candidates using PCM may be divided into three major steps: (i) tracking of charged particles and secondary vertex, V^0, finding [34]; (ii) particle identification and (iii) photon candidate reconstruction and subsequent selection. The secondary vertices used in this analysis were obtained during data reconstruction using all available tracking information, calculating the momenta of the daughter tracks with respect to the secondary vertex. The tracks associated with secondary vertices were required to have a momentum of at least $p_{\rm T}^{\rm track} > 50$ MeV/c and at minimum 60% of findable TPC clusters. In order to reduce contamination from Dalitz decays, conversion candidates were only considered with a vertex at a radial distance of at least $R > 5$ cm. In addition, a line-cut was applied to restrict the geometrical η distribution of the conversion points with the nominal center of the detector as origin. This cut removed photon candidates that would otherwise appear outside the angular dimensions of the detector. The condition $R_{\rm conv} > |Z_{\rm conv}| S_{\rm ZR} - 7$ cm was applied with

$S_{\mathrm{ZR}} = \tan(2\arctan(\exp(-\eta_{\mathrm{cut}})))$ and $\eta_{\mathrm{cut}} = 0.9$, where the coordinates R_{conv} and Z_{conv} were determined with respect to the center of the detector. Additional constraints were imposed on $R_{\mathrm{conv}} < 180$ cm and $|Z_{\mathrm{conv}}| < 240$ cm to ensure that the reconstruction of secondary tracks was performed inside the TPC. Electrons and positrons from photon conversions were identified via their energy deposit in the TPC ($\mathrm{d}E/\mathrm{d}x$). The difference of the measured $\mathrm{d}E/\mathrm{d}x$ value from the hypothesis of the electron/positron energy loss was used for the particle identification. The $\mathrm{d}E/\mathrm{d}x$ of measured charged tracks was required to be within $-3 < \mathrm{n}\sigma_{\mathrm{e}} < 5$ of the expected energy loss, where σ_e is the Gaussian width of the measured $\mathrm{d}E/\mathrm{d}x$ distribution and is momentum dependent. To further reduce charged pion contamination as the pion $\mathrm{d}E/\mathrm{d}x$-band begins to merge with the electron/positron $\mathrm{d}E/\mathrm{d}x$-band above $p \gtrsim 4$ GeV$/c$, a cut based on the separation from the hypothesis of charged pion energy loss was applied in $n\sigma_{\pi}$. Tracks with energy losses closer to the pion line than $|n\sigma_{\pi}| < 1$ were removed; this is done for PCM only up to 3.5 GeV$/c$. The non-photon V^0 candidate contamination was further suppressed by a triangular two-dimensional cut, $|\Psi_{\mathrm{pair}}| < \Psi_{\mathrm{pair,max}}(1-\chi^2_{\mathrm{red}}/\chi^2_{\mathrm{red,max}})$, with $\chi^2_{\mathrm{red,max}} = 30$ and $\Psi_{\mathrm{pair,max}} = 0.1$. This cut is based on the reduced χ^2 of the Kalman-Filter [36] hypothesis for the e^+e^- pair and on the angle Ψ_{pair} between the plane perpendicular to the magnetic field of the ALICE magnet and the e^+e^- pair plane. Furthermore, a cut on the cosine of the pointing angle of $\cos(\theta_{\mathrm{PA}}) > 0.85$ was performed, where the pointing angle, θ_{PA}, is the angle between the reconstructed photon momentum vector and the vector joining the collision vertex. The remaining $\mathrm{K}^0_{\mathrm{S}}$, Λ and $\overline{\Lambda}$ contamination was removed by selecting $q_{\mathrm{T}} < q_{\mathrm{T,max}}\sqrt{1-\alpha^2/\alpha^2_{\mathrm{max}}}$ on the Armenteros-Podolanski plot [37] with $q_{\mathrm{T,max}} = 0.05$ GeV$/c$ and $\alpha_{\mathrm{max}} = 0.95$. Additionally, the PCM measurement requires an out-of-bunch pileup correction which estimates the contamination of photon candidates from multiple events overlapping in the TPC. The correction is based on a study of the distance of closest approach (DCA) of the conversion photon candidates which is the smallest distance in beam direction (z) between the primary vertex and the momentum vector of the photon candidate. Photon candidates from different events generate a broad underlying Gaussian-like DCA distribution, which was fitted in order to estimate the out-of-bunch pileup contribution. The correction was found to be p_{T} dependent and ranged from 42% at low $p_{\mathrm{T}} \approx 0.35$ GeV$/c$ to 10% at high $p_{\mathrm{T}} \approx 11$ GeV$/c$.

The hybrid PCM-EMCal method used the same cuts on photon candidates as the respective standalone reconstruction methods. Only the upper value of the cut on the short axis of the moment of the shower shape for the EMCal is changed and required to be $\sigma^2_{\mathrm{long}} \leq 0.5$ in order to further reject contamination of hadrons. Due to the timing constraint of EMCal restricting clusters to triggered bunch crossings, no DCA or additional out-of-bunch pileup rejection was needed for the hybrid method. In addition to the general matching of primary charged particles to EMCal clusters already described, a dedicated track matching procedure for the two charged V^0 daughters with respect to EMCal clusters was applied. This cluster-V^0 track matching was the most important ingredient for the hybrid analysis, as pairing one leg of the V^0 candidate with the EMCal cluster generated by one of those secondary charged tracks itself, leads to an auto-correlation and causes a broad peak between the masses of the π^0 and η mesons at around 300 MeV/c. The same parameters from the general track matching procedure were found to remove 99% of such candidates.

The invariant mass of two photon candidates was determined by adding the respective four-momentum vectors and squaring the resulting vector, yielding the invariant mass of the parent particle which is independent of the reference system. Invariant mass distributions include combinatorial background as well as the signal for photon candidate pairs from the same event. The uncorrelated combinatorial background was estimated by using an event mixing technique [38], in which photon candidates from different events were paired in order to prevent correlations between the candidates. An opening angle cut of 17 mrad for the angle between the momentum vectors of the two paired photon candidates was applied for the EMCal di-cluster measurement. Requiring such a minimum separation between clusters is needed to ensure a proper background description by event mixing [38], in which two clusters from different events might otherwise be separated by an arbitrarily small distance. In same events, such cluster configurations would overlap partially or even merge into single clusters, which has been explicitly considered

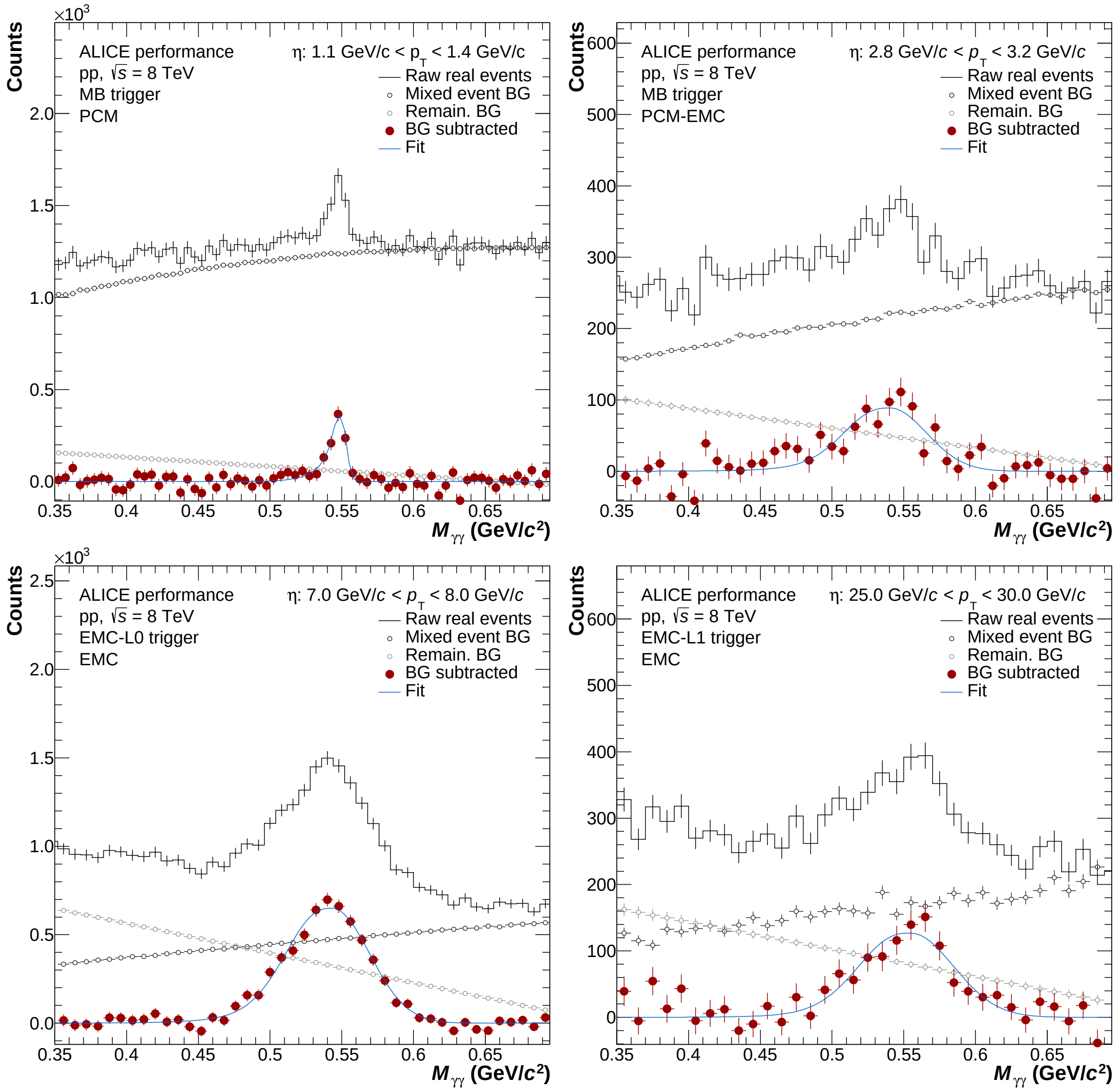

Fig. 3: Example invariant mass spectra in selected p_{T} slices in PCM (top left), PCM-EMCal (top right) and EMCal (bottom plots) in the η mass region. The black histograms show invariant mass distributions before any background subtraction. The grey points show mixed event and residual correlated background contributions, which have been subtracted from raw real events to obtain the signal displayed with red data points. The blue curves represent fits to the background subtracted invariant mass spectra.

for event mixing by not allowing the cells with largest deposited energies of respective clusters to be neighbors on EMCal surface. For the PCM and hybrid PCM-EMCal method, an opening angle cut of 5 mrad was further applied between the momentum vectors of the pair of conversion photon candidates and accordingly, the PCM and EMCal photon candidates.

The mixed event background distribution was scaled to match the raw signal distribution in the vicinity of the peak region, after which it was subtracted from the raw signal. For the π^0 meson measurement with the PHOS, invariant mass distributions from event mixing were multiplied by first or second order polynomial functions to estimate uncorrelated and remaining background contributions. The mixed event background subtracted signal was fitted to determine the mass peak position and width of π^0 and η mesons. The PHOS invariant mass spectra were fitted using a Crystal Ball function [39]. For the EMCal, PCM and hybrid PCM-EMCal cases, a Gaussian function combined with an exponential low mass tail was used [40]. These two functions have a tail on the low mass side to account for late conversions of one or both gammas in PHOS and EMCal analyses and to account for energy loss effects due to bremsstrahlung in the PCM and hybrid PCM-EMCal analyses. To reflect residual correlated background components, which remain after the subtraction of mixed event background, the fitting of peaks was performed including an additional first order polynomial function. Example invariant mass spectra with π^0 and η meson candidates are shown in Figs. 2 and 3, illustrating the meson reconstruction over the full p_{T} range reported in this analysis.

The measurement of neutral pions using the EMCal has a natural upper limit of the order of $p_{\mathrm{T}}^{\pi^0} \approx$ 20 GeV/c due to the segmentation of cells. As the opening angles of the two decay photons become smaller with increasing transverse momenta due to the Lorentz boost, a larger percentage of showers produced by π^0 decay photons merge into single clusters. While the dominant symmetric decays are first to merge, the asymmetric decay contributions become more relevant at higher momenta. Above a certain limiting momentum, it is no longer possible to separate the two decay photons of the π^0, creating merged clusters that significantly reduce the reconstruction efficiency in the EMCal as seen in Fig. 5. In contrast, the PCM-EMCal hybrid approach overcomes the limitations of the EMCal cell segmentation and makes it possible to reconstruct neutral pions up to a transverse momentum of 35 GeV$/c$ as reported in this paper. As the opening angles of photons from η decays are larger than those of neutral pions, the merging of clusters sets in at much higher momentum. Hence, the EMCal measurement of η mesons is feasible up to highest reported transverse momenta of 35 GeV/c where lack of statistics is still the limiting factor. For the PHOS, the cluster merging effect sets in much later, as the dimensions of single readout cells is $\sim$7 times smaller than those of the EMCal, as described in Sec. 2. It becomes significant for the PHOS only beyond the reported measurement interval.

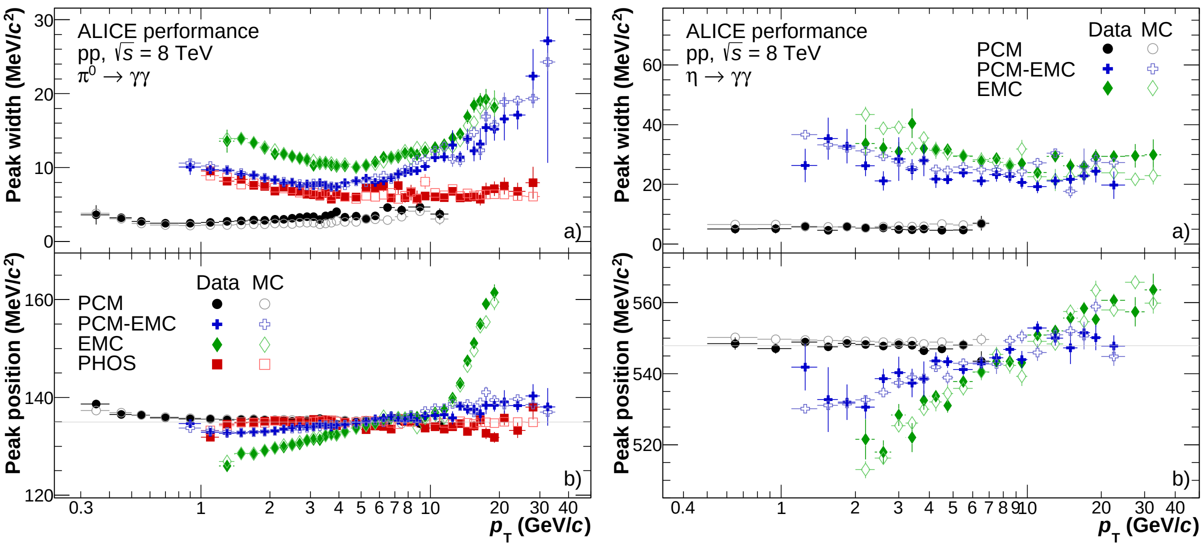

Fig. 4: The left plots show reconstructed π^0 peak positions (left-bottom) and widths (left-top) of each reconstruction method compared to MC simulations for the transverse momentum bins used in the analysis. Corresponding plots for the η meson are on the right for peak masses (right-bottom) and widths (right-top).

The raw yields of neutral mesons were obtained by integrating the background-subtracted invariant mass distributions around the reconstructed meson masses. These mass positions were extracted from the respective fits of the signal peaks. The mass positions together with the reconstructed meson peak widths defined the integration ranges for calculating the raw yields in a given p_{T} bin. The reconstructed π^0 and η meson mass peak positions and widths as a function of p_{T} for each reconstruction method were compared to full detector GEANT3 [41] MC, Fig. 4, which realistically simulate interactions between the particles and the detector material. In the PHOS analysis, the π^0 integration range was asymmetrically defined as $[-5\sigma, +3\sigma]$ where σ is the standard deviation of the Gaussian part of the fitting function. For each of the analysis methods and triggered datasets analysed, the integration windows for both neutral mesons was chosen to cover at least three sigmas of the reconstructed peak width around the reconstructed meson masses on both sides.

Corrections for geometrical acceptance and reconstruction efficiencies were evaluated using MC simulations. PYTHIA8 [16] and PHOJET [42] event generators with minimum bias processes were used. The correction factors for both MC productions were found to be consistent and, hence, were combined. For mesons with $p_{\mathrm{T}} > 5$ GeV$/c$, thus in particular for the triggered datasets, a PYTHIA8 simulation was used that was enriched with jets, generated in bins of hard scatterings, $p_{T,\mathrm{hard}}$. Particles generated by the event generator were propagated through the ALICE detector and were simulated by GEANT3 [41]. In the simulation, the same reconstruction algorithms and analysis cuts were applied as those used to obtain the yields for real data. In Fig.4, the reconstructed π^0 and η peak positions and widths were compared between data and MC to confirm a proper detector response in the simulation. The calculated correction factors, ε, for each method, containing the specific detector acceptances as well as full reconstruction efficiencies, are shown in Fig. 5, where the acceptance correction is further normalized to unit rapidity and azimuth angle to enable a direct comparison between the different methods. For the EMCal analysis, the correction factors are observed to decrease at high transverse momenta for $p_{\mathrm{T}} \gtrsim 10$ GeV$/c$. This is due to the effect of cluster merging where the opening angle of the neutral pions becomes too small to resolve adjacent clusters due to the finite segmentation of the calorimeter.

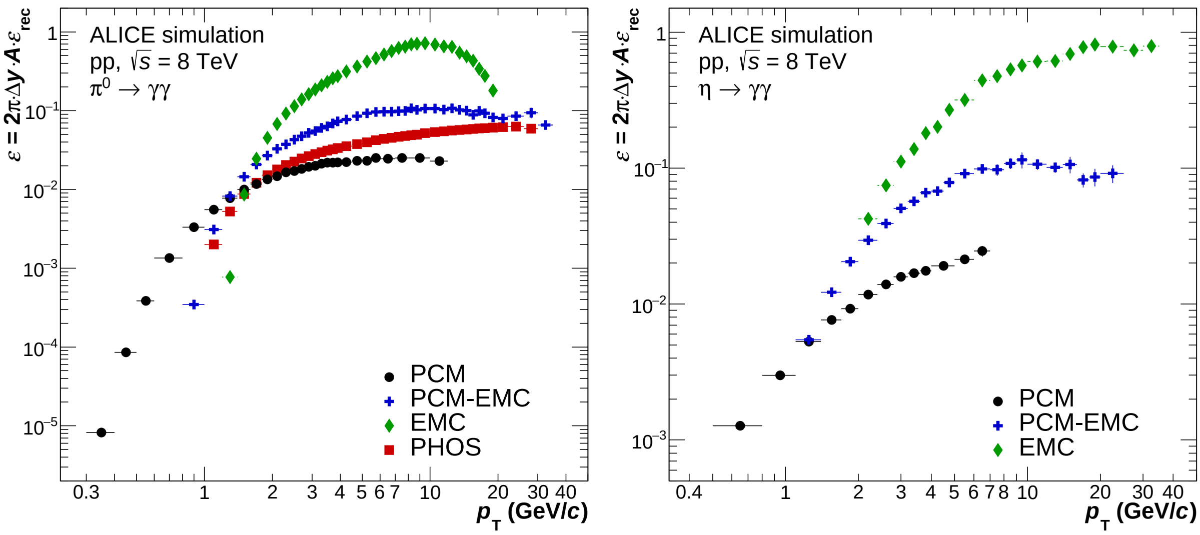

Fig. 5: The total correction factors, ε, for each reconstruction method for π^0 (left) and η mesons (right) plotted versus transverse momentum bins used in the analysis. The factors contain detector acceptances and respective reconstruction efficiencies, where acceptances are further normalized to rapidity, y, and polar angle, φ.

For π^0 measurements, contributions of secondary neutral pions from weak decays and hadronic interactions were estimated and removed. Weak decays of $\mathrm{K^0_S}$ represent the main source of secondaries. For all reconstruction methods, the spectra of the three main particles relevant for the secondary neutral pion correction due to weak decays, $\mathrm{K^0_S}$, $\mathrm{K^0_L}$ and Λ, were obtained from [43–45] with extrapolation of spectra to 8 TeV, assuming a power law for each p_{T} bin as function of $\sqrt{s}$. Using a decay photon cocktail simulation, the decay of those particles was simulated, and their raw yields were fed into the correction procedure. The contributions from the remaining secondary pions, for example due to interactions with detector material, were obtained purely from MC, which is the only viable approach. From the MC simulations, the acceptance and reconstruction efficiencies for secondary pions from the various sources were calculated, and multiplied with the obtained raw yields, in order to obtain the secondary corrections, which are of the order of 1-3% for $\mathrm{K^0_S}$, <0.5% for $\mathrm{K^0_L}$, $\lesssim$0.02% for Λ and 0.1-2% for material pions, varying within the given values for the different methods and triggers used.

As there are three different triggers available for the EMCal and hybrid PCM-EMCal methods, and two different ones for the PHOS measurement, each with its own statistical and systematic uncertainties, as well as correlations between the different systematical uncertainties, the results from each trigger class were properly combined in order to obtain the final result for each reconstruction method. Statistical uncertainties were ensured to be uncorrelated since different triggers use non-overlapping data samples. For the systematic uncertainties, the transverse momentum dependent correlation coefficients were determined. Only a few systematic uncertainties were found to be uncorrelated, such as the uncertainty of signal extraction and partly "efficiency" and "trigger" related uncertainties, for which further details are contained in Sec. 5. The correlation coefficients were found to be generally above 0.8. The respective p_{T} dependent weights were calculated according to the BLUE algorithm [46–50], which were used to combine the spectra from each method.

5 Systematic uncertainties

Systematic uncertainties are respectively summarized in Tabs. 2, 3 and 4 for the neutral mesons π^0, η and their ratio η/π^0. The values are given in percent and refer to relative systematic uncertainties of the measured values. Three different example p_{T} bins are listed for each reconstruction method in order to illustrate their relative strengths. An additional, more detailed description of the systematic sources and the determination of uncertainties for all methods except PHOS may be found in [9], which is fully applicable to this paper.

p_{T} interval	1.4 – 1.6 GeV/c				5.0 – 5.5 GeV/c				15.0 – 16.0 GeV/c		
Method	PCM	PCM-EMC	EMC	PHOS	PCM	PCM-EMC	EMC	PHOS	PCM-EMC	EMC	PHOS
Signal extraction	4.8	1.9	2.3	3.0	5.4	2.4	1.5	1.8	3.3	4.6	1.0
Inner material	9.0	4.5	-	-	9.0	4.5	-	-	4.5	-	-
Outer material	-	4.2	4.2	3.5	-	4.2	4.2	3.5	4.2	4.2	3.5
PCM track rec.	1.0	0.5	-	-	1.0	0.9	-	-	2.1	-	-
PCM electron PID	1.8	0.6	-	-	1.1	1.4	-	-	3.1	-	-
PCM photon PID	1.7	0.5	-	-	2.1	1.1	-	-	3.5	-	-
Cluster description	-	2.5	4.4	-	-	2.5	3.7	-	4.3	4.0	-
Cluster energy calib.	-	1.8	2.5	2.6	-	1.9	1.8	0.6	2.8	2.0	0.6
Track match to cluster	-	0.2	3.1	-	-	0.5	2.1	-	3.3	3.7	-
Efficiency	-	2.0	2.0	5.5	-	2.9	2.4	5.5	2.7	3.5	7.5
Data taking periods	3.0	3.0	3.0	4.3	3.0	3.0	3.0	4.3	3.0	3.0	-
Trigg. norm.&pileup	3.4	0.1	0.1	1.2	2.2	0.8	0.5	1.2	2.3	2.4	12.5
Total syst. uncertainty	11.5	8.1	8.4	8.9	11.4	8.7	7.5	8.2	11.6	10.0	15.0
Statistical uncertainty	1.5	1.5	3.4	7.2	8.4	3.2	2.0	8.2	8.0	4.5	10.6

Table 2: Summary of relative systematic uncertainties in percent for selected p_{T} bins for the reconstruction of π^0 mesons. The statistical uncertainties are given in addition to the total systematic uncertainty for each bin. The uncertainty from $\sigma_{\mathrm{MB_{AND}}}$ determination of 2.6%, see [32], is independent from reported measurements and is separately indicated in plots below.

For the measurement of neutral pions by PHOS, the systematic uncertainty related to signal extraction was evaluated by varying the fitting range and the assumptions about the mass peak and background shapes. The systematic uncertainty related to the material budget was taken from [3], which was estimated by comparing the results of the analysis with and without magnetic field in the ALICE solenoid. Photons, which converted to e^+e^- pairs within the detector material, are most likely being reconstructed as two clusters in the presence of a magnetic field. Without a field, the secondary tracks from photon conversions are less separated and can be dominantly detected as single clusters, building the correct invariant masses for neutral pions in di-cluster analyses. Therefore, comparing the π^0 spectra from data and MC with nominal and zero magnetic fields is a straightforward method to evaluate the uncertainty of the material budget description in simulations. Systematic uncertainties due to the cluster energy calibration were decomposed into the uncertainty of the energy scale of clusters and non-linearity effects. The energy scale uncertainty of 0.1% was estimated from a comparison of the π^0 mass peak position for the two-photon invariant mass spectra in data and MC. This energy uncertainty was translated to an uncertainty of the π^0 yield by convolution with the shape of the p_{T}-spectrum. The systematic uncertainty due to non-linearity correction was evaluated by introducing different non-linearity correction schemes and calibration parameters for the MC simulation, whereas the p_{T} dependence of the π^0 peak position and width was always kept consistent with data. The efficiency uncertainty consists of acceptance variations and differences between MC event generators. The acceptance uncertainty was estimated by changing the good cluster selection criteria, and the MC generator dependent uncertainty was evaluated by comparing efficiencies of minimum bias MC generators and single particle MC simulation which generates events with single neutral mesons with realistic transverse momentum and rapidity distributions. Moreover, it included the trigger efficiency uncertainty in the high energy photon trigger analysis. It was estimated by comparing the trigger turn-on curve from data with MC simulations. In the PHOS minimum bias analysis, three different data taking periods were used, in which the variations in the neutral meson spectra were not fully covered by statistical fluctuations. To reflect these biases, the corresponding uncertainty denoted "data taking period" was evaluated by comparison of the full corrected spectra of each period. "Trigger normalization & pileup" summarizes systematic uncertainties due to the trigger normalization factor and pileup effects. The uncertainty related to the trigger normalization factor was estimated by changing the range of the fit to determine the rejection factor. Furthermore, the out-of-bunch pileup contribution was evaluated by varying the timing cut to accept clusters.

p_{T} interval	2.0 – 2.4 GeV/c			5.0 – 6.0 GeV/c			18.0 – 20.0 GeV/c	
Method	PCM	PCM-EMC	EMC	PCM	PCM-EMC	EMC	PCM-EMC	EMC
Signal extraction	5.1	9.0	9.2	7.3	7.3	6.0	10.6	7.8
Inner material	9.0	4.5	–	9.0	4.5	-	4.5	-
Outer material	-	4.2	4.2	-	4.2	4.2	4.2	4.2
PCM track rec.	1.5	1.8	-	2.0	2.4	-	3.3	-
PCM electron PID	2.4	1.8	-	2.2	2.9	-	6.5	-
PCM photon PID	3.6	2.9	-	6.3	3.0	-	7.9	-
Cluster description	-	3.1	4.6	-	4.0	4.9	6.0	4.9
Cluster energy calib.	-	3.2	3.5	-	3.9	3.5	4.5	3.5
Track match to cluster	-	1.5	4.0	-	1.7	3.2	4.2	3.3
Efficiency	-	5.0	4.0	-	9.8	5.3	10.0	6.0
Data taking periods	3.0	3.0	3.0	3.0	3.0	3.0	3.0	3.0
Trigg. norm.&pileup	2.1	0.1	0.1	1.4	1.5	1.5	3.0	2.7
Total syst. uncertainty	11.9	13.8	13.3	14.0	16.0	11.8	21.4	13.3
Statistical uncertainty	10.4	12.1	16.7	19.6	6.8	5.0	21.3	8.3

Table 3: Summary of relative systematic uncertainties in percent for selected p_{T} bins for the reconstruction of η mesons, see Tab. 2 for further explanations which also apply here.

For the PCM measurement, the main source of systematic uncertainty is the material budget, for which we used the same value previously calculated in [3]. The signal extraction uncertainty was estimated by changing the integration window around the invariant mass peak, the normalization range of the combinatorial background and by using different combinatorial background evaluation schemes. "Track reconstruction" summarizes the systematic uncertainties found by requiring different number of TPC clusters and minimum transverse momentum cuts on tracks. The systematic uncertainties due to electron identification ("electron PID" and "PCM photon PID") were determined by varying the PID cuts, as described in Sec. 4, and by comparing the respective results. As the analyzed data for PCM, PCM-EMCal and EMCal is composed of seven different data taking periods, the corresponding uncertainty denoted as "data taking periods" reflects the associated systematics. It was evaluated by running the analyses separately for each period and comparing the results. For PCM, the "trigger normalization & pileup" uncertainty is dominated by the uncertainty of the DCAz background description for the out-of-bunch pileup estimation. Furthermore, it contains the systematic uncertainty due to pileup rejection by SPD due to its finite efficiency to remove pileup events.

For the EMCal, one main systematic uncertainty arises from the knowledge of the outer material budget, which is defined by all detector components from the radial center of the TPC up to the EMCal. The uncertainty was assessed by running the analysis only with/without TRD modules in front of the EMCal, since part of the data taking in 2012 occurred with the EMCal only partially obscured by the TRD. Since material budgets are similar between TRD and TOF, the same uncertainty has been assigned to TOF as it covered full polar angle so that a similar assessment was not feasible. Both uncertainties were quadratically combined to arrive at the given uncertainties. The signal extraction uncertainty contains the systematic uncertainties obtained from variations of background normalization region, the choice of background fit function and integration intervals, as well as from variations of the minimum meson opening angle cut. The uncertainty denoted by "cluster description" summarizes the systematic uncertainties due to the cluster description in the MC, giving rise to modified reconstruction efficiencies, which includes the following cluster related quantities: minimum energy, shower shape, number of cells, time and clusterization seed as well as minimum energy cut variations. Moreover, cell timing cut variations are also included in this category. "Cluster energy calibration" considers the systematic uncertainties due to non-linearity effects and the energy scale of clusters. Different non-linearity schemes were used in this analysis from which this uncertainty was obtained. Moreover, the energy scale uncertainty was determined by obtaining the residual difference of meson mass positions between data and MC simulations. The systematic uncertainty induced by the matching of charged particles to clusters and the subsequent removal of such cluster candidates was determined by varying the matching residuals. The "efficiency" uncertainty reflects differences between minimum bias MC generators for efficiency calculation. Moreover, it contains the uncertainty of the actual trigger turn-on as described by MC simulation. The uncertainty reflected by "data taking periods" was determined according to the description from the previous PCM related paragraph. It was evaluated by separately running the analysis for each data taking period and comparing the results. The "trigger normalization & pileup" uncertainty summarizes the uncertainty of the determination of trigger rejection factor as well as the systematic uncertainty due to pileup rejection by SPD which has a finite efficiency for pileup removal.

p_{T} interval	2.0 – 2.4 GeV/c			5.0 – 6.0 GeV/c			18.0 – 20.0 GeV/c	
Method	PCM	PCM-EMC	EMC	PCM	PCM-EMC	EMC	PCM-EMC	EMC
Signal extraction	5.9	9.0	9.3	8.2	7.5	6.6	11.2	12.7
PCM track rec.	1.5	1.9	-	2.0	2.4	-	3.8	-
PCM electron PID	2.4	1.9	-	2.2	3.5	-	7.4	-
PCM photon PID	3.6	3.2	-	6.3	3.6	-	9.0	-
Cluster description	-	3.5	4.9	-	4.1	5.2	8.9	5.5
Cluster energy calib.	-	3.4	4.2	-	4.6	4.3	5.5	4.5
Track match to cluster	-	1.5	4.0	-	1.8	3.2	6.1	3.3
Efficiency	-	5.4	4.5	-	9.8	5.9	10.5	7.4
Total syst. uncertainty	7.5	12.4	12.8	10.8	15.0	11.5	23.1	16.7
Statistical uncertainty	11.3	12.2	5.2	20.0	7.4	2.8	23.3	17.3

Table 4: Summary of relative systematic uncertainties in percent for selected p_{T} bins for the determination of η/π^0 ratio. The statistical uncertainties are given in addition to the total systematic uncertainty for each bin.

For the hybrid method PCM-EMCal, the same cut variations were performed as for the standalone methods. However, given the fact that only one photon candidate of each system was used, most systematic uncertainties were found to be of different size or behavior, e.g. the minimum opening angle cut variations. The "track matching to cluster" uncertainty reflects the V^0-track to cluster matching which is of crucial importance for the hybrid system, as described in Sec. 4. The uncertainty was assessed by varying the matching residuals.

As indicated in Tab. 4, many uncertainties cancel for the η/π^0 ratio, such as the material-related systematics. For the remaining categories, the respective uncertainties of neutral pion and η measurements were added quadratically and canceled partially beforehand, if applicable.

6 Results

The invariant differential cross sections of π^0 and η production were obtained from the number of reconstructed mesons $N^{\pi^0(\eta)}$ by applying all necessary corrections using the following expression:

$$E\frac{\mathrm{d}^3\sigma^{pp\to\pi^0(\eta)+X}}{\mathrm{d}p^3} = \frac{1}{2\pi p_{\mathrm{T}}}\frac{1}{\mathscr{L}_{\mathrm{int}}}\frac{1}{A\cdot\varepsilon_{\mathrm{rec}}}\frac{1}{Br_{\pi^0(\eta)\to\gamma\gamma}}\frac{N^{\pi^0(\eta)}-N^{\pi^0}_{\mathrm{sec}}}{\Delta y\Delta p_{\mathrm{T}}}, \tag{2}$$

where $N^{\pi^0}_{\mathrm{sec}}$ only applies for the neutral pion and represents the estimated number of secondaries, $\mathscr{L}_{\mathrm{int}}$ is the integrated luminosity as mentioned in Sec. 3, $A\cdot\varepsilon_{\mathrm{rec}}$ is the product of the geometrical acceptance and reconstruction efficiency, also referred to as ε, see Fig. 5, $Br_{\pi^0(\eta)\to\gamma\gamma}$ is the branching ratio for the two-gamma decay channel and $\Delta y\Delta p_{\mathrm{T}}$ is the bin width in rapidity and transverse momentum. For the measurement of neutral pions by PCM, the out-of-bunch pileup correction has to be noted for completeness and to be applied as well.

The invariant differential cross sections were independently measured with each method. The final spectra were obtained by combining the results in the overlap regions using the previously mentioned BLUE method [46–50] from Sec. 4, properly taking into account the correlations of the systematic uncertainties of the different reconstruction methods. Possible statistical correlations between the measurements, for instance due to the conversions at small distances relative to the beam axis, are negligible due to the small conversion probability and the small likelihood of reconstructing the respective electron in the calorimeters leading to a meson candidate which finally ends up in the respective integration window. As there are no common uncertainties present for PCM, EMCal and PHOS, all systematic uncertainties were considered to be completely uncorrelated in those cases. On the other hand, the correlations introduced by including the hybrid PCM-EMCal measurement had to be taken into account. By construction, there are different numbers of conversion photons entering the two methods. Thus, all systematic uncertainty sources from PCM are found to be partially correlated in the PCM-EMCal method. Half of the size of the material budget uncertainty, for example, is assumed to be uncorrelated. Furthermore, the uncorrelated systematic uncertainties from PCM-EMCal with respect to PCM are, with full size, all the calorimeter related uncertainties as well as trigger and efficiency uncertainties.

Due to finite bin widths of the measured production cross sections, every reported spectrum was shifted accordingly in x-coordinates [51]. All bin width corrections are of the order of 1% and below. In contrast, the reported η/π^0 ratios are shifted in y-coordinates, as otherwise the ratio could not be computed and the different measurements could not be combined. The correction is below 1% for $p_{\mathrm{T}} > 2$ GeV/c, but becomes significant for smaller momenta and rises to 8% for the lowest bin.

The combined invariant cross sections of inclusive π^0 and η meson production cover transverse momentum ranges of $0.3 < p_{\mathrm{T}} < 35$ GeV/c and $0.5 < p_{\mathrm{T}} < 35$ GeV/c, respectively. They are shown in Fig. 7. Both combined spectra of π^0 and η mesons were fitted to the two-component model (TCM) proposed in [52] by using the total errors on spectra, obtained by quadratically combining statistical and systematic uncertainties. Its functional form is a combination of a Boltzmann component and a power-law part, which, in general, should be the dominant components at low and high p_{T}, respectively. The fit function is able to reproduce the spectrum over the full p_{T} range and is described as

$$E\frac{\mathrm{d}^3\sigma}{\mathrm{d}p^3} = A_{\mathrm{e}}\exp\left(-E_{\mathrm{T,kin}}/T_{\mathrm{e}}\right) + A\left(1+\frac{p_{\mathrm{T}}^2}{T^2 n}\right)^{-n}, \tag{3}$$

where $E_{\mathrm{T,kin}} = \sqrt{p_{\mathrm{T}}^2 + m^2} - m$ is the transverse kinematic energy of the meson, with m being the rest mass of the meson, A_{e} and A are the normalization factors, T_e, T and n are free parameters. For a comparison between the measurements, the ratios of spectra measured by each reconstruction system to the TCM fit of the combined spectrum are shown in Fig. 6.

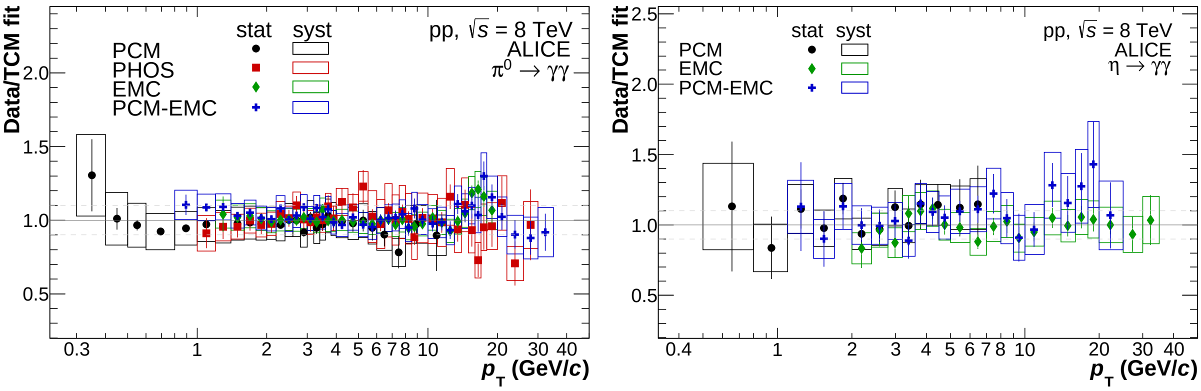

Fig. 6: Ratios of the fully corrected π^0 (left) and η (right) spectra for each reconstruction method to the TCM fit of the combined spectrum.

The vertical error bars represent the statistical uncertainties and the boxes quantify the systematic errors. All measurements agree within uncertainties over the whole p_{T} range.

The reported measurements were also fitted with a Levy-Tsallis function [53], which has been used in previous measurements of π^0 and η spectra in pp collisions by ALICE [3, 4]

$$E\frac{\mathrm{d}^3\sigma}{\mathrm{d}p^3} = \frac{C}{2\pi}\frac{(n-1)(n-2)}{nT(nT+m(n-2))}\left(1+\frac{m_{\mathrm{T}}-m}{nT}\right)^{-n}, \tag{4}$$

where C, n and T are free parameters of the fit. The fit parameters extracted from both the TCM and Levy-Tsallis fits are summarized in Tab. 5. Combined statistical and systematic uncertainties were used in the fitting process. The TCM is chosen as the standard fit function, since it better describes the spectra at low and high p_{T} than the Levy-Tsallis counterpart. This is reflected in the smaller values obtained for the reduced χ^2_{red} of the respective fits, which are also recorded in Tab. 5. A direct comparison of TCM and Levy-Tsallis fits can be found in Fig. 7, where both fits are plotted, in addition to the measured spectra and theory calculations.

TCM	A_e (pb GeV$^{-2}c^3$)	T_e (GeV)	A (pb GeV$^{-2}c^3$)	T (GeV)	n	χ^2_{red}
π^0	$(6.69\pm2.74)\times10^{11}$	0.144 ± 0.021	$(3.44\pm0.92)\times10^{10}$	0.604 ± 0.033	3.028 ± 0.019	0.27
η	$(1.48\pm4.51)\times10^{9}$	0.225 ± 0.234	$(2.98\pm1.90)\times10^{9}$	0.805 ± 0.104	3.041 ± 0.046	0.32

Levy-Tsallis	C (pb)	T (GeV)	n	χ^2_{red}
π^0	$(2.44\pm0.18)\times10^{11}$	0.121 ± 0.004	6.456 ± 0.043	0.48
η	$(1.56\pm0.19)\times10^{10}$	0.220 ± 0.012	6.559 ± 0.116	0.58

Table 5: Parameters of the fits to the π^0 and η invariant differential cross sections using the TCM fit [52] from Eq. 3 as well as using a Levy-Tsallis fit [53] from Eq. 4.

The measured invariant cross sections were compared with NLO pQCD calculations using MSTW08 PDF [13] plus DSS14 FF [8] for π^0 and CTEQ6M5 PDF[14] plus AESSS FF [15] for the η meson. The same factorization scale value, μ, $(0.5p_{\mathrm{T}} < \mu < 2p_{\mathrm{T}})$ was chosen for the factorization, renormalisation and fragmentation scales used in the NLO pQCD calculations. In the case of π^0, the NLO PDF and

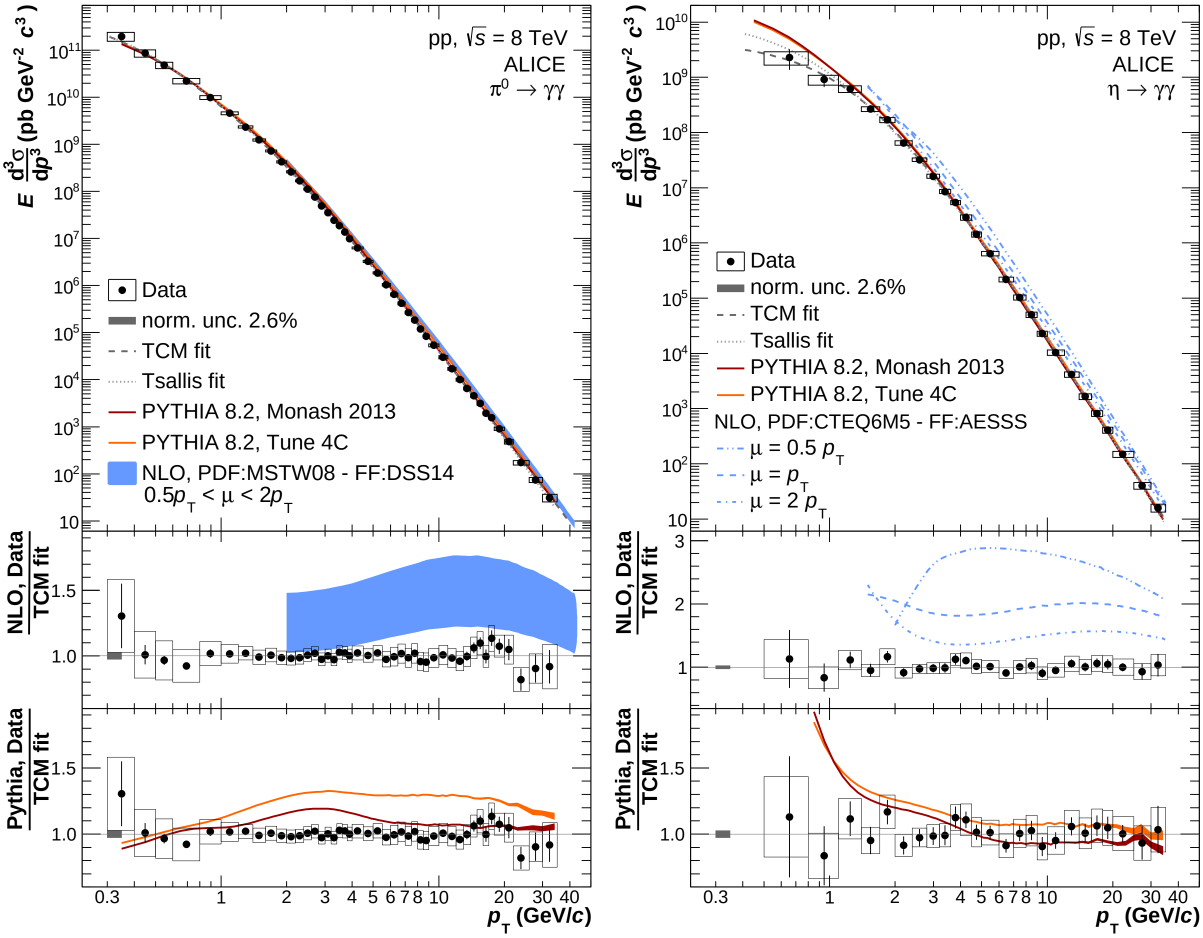

Fig. 7: Invariant cross sections for neutral meson production shown together with NLO pQCD predictions using PDFs MSTW08 (CTEQ6M5) with FFs DSS14 (AESSS) for π^0 (η) as well as PYTHIA8.210 calculations, for which two different tunes were available. The data points were fitted using a TCM fit, Eq. 3, and a Levy-Tsallis fit, Eq. 4.

pQCD plus FF combination describes the RHIC data rather well [54], whereas for $\sqrt{s} = 2.76$ TeV pQCD overpredicts ALICE data by 30% at moderate p_{T} and agrees at higher p_{T} [9]. The ratios of data and NLO pQCD predictions to the TCM fits of neutral meson spectra are shown in Fig. 7. The largest uncertainty of the NLO pQCD calculation is due to the choice of μ. For all μ values, these calculations overestimate the measured data for both π^0 and η mesons. This was also observed for meson measurements at $\sqrt{s} = 2.76$ TeV by ALICE [9], although better description of data is achieved for $\mu = 2p_{\mathrm{T}}$, for which calculations are above data by $10-40\%$ depending on p_{T}. It has to be noted that FF uncertainties of NLO pQCD calculations have been considerably reduced after including the published π^0 measurement at $\sqrt{s} = 7$ TeV [3] for DSS14. Including precise new data for η meson production measured at $\sqrt{s} = 2.76$, 7 and 8 TeV [3, 9] will also help to considerably reduce NLO pQCD uncertainty bands in that case. In addition, the reported neutral meson measurements at $\sqrt{s} = 8$ TeV were compared to PYTHIA8.210 [16] references; Tune 4C [17] and Monash 2013 tune [18]. To enable a proper comparison of the PYTHIA tunes with the measured neutral meson spectra, π^0 mesons from decays of long-living strange particles (K^0_S, Λ, Σ and Ξ) were excluded. The Tune 4C calculation is about 30% above the π^0 measurement for $p_{\mathrm{T}} > 1.5$ GeV$/c$. In contrast, the Monash 2013 tune reproduces the neutral pion spectrum within 10% for almost the complete transverse momentum range, although both tunes are not able to describe the shape of the measured spectrum indicated by the bump at approximately 3 GeV$/c$. Concerning the η meson, both tunes reproduce the measured spectrum for $p_{\mathrm{T}} > 1.5$ GeV$/c$ within uncertainties. At lower momenta $p_{\mathrm{T}} < 1.5$ GeV$/c$, both tunes follow the same trend and deviate significantly in magnitude and shape from data. The tuning parameters of the soft QCD part of PYTHIA apparently fail to describe the measured η meson spectrum below $p_T < 1.5$ GeV/c, whereas there is further tension up to $p_T \approx 3.5$ GeV/c. On the other hand, both PYTHIA tunes are consistent within uncertainties with the measured π^0 spectrum for the low transverse momentum interval $0.3 < p_T < 1.5$ GeV/c.

The mean transverse momenta, $\langle p_T \rangle$, were determined for the neutral meson spectra shown in Fig. 7. Three different fit functions were used in this context: a TCM, Eq. 3, a Tsallis, Eq. 4, and a modified Hagedorn [55] fit that was used as the default fit function. The obtained values for the π^0 and η mesons are listed in Tab. 6, where statistical and systematic uncertainties are quoted. The additional uncertainty term denoted with "fit sys" reflects the choice of the fitting function. Moreover, the introduced fit functions were also used to calculate the integrated yields, $\mathrm{d}N/\mathrm{d}y$, for both neutral mesons in inelastic events. The cross section for inelastic pp collisions at $\sqrt{s} = 8$ TeV, $\sigma_{\mathrm{INEL}} = 74.7 \pm 1.7$ mb [56], was used for this purpose. The obtained yields are given in Tab. 6, which are based on extrapolation fractions, F_{extpol}, of about 46% for the π^0 and about 33% for the η meson. Additionally, the integrated η/π^0 ratio was estimated and can be found in Tab. 6 as well. For the recent paper by ALICE on neutral meson production in pp collisions at $\sqrt{s} = 2.76$ TeV [9], the mean p_T as well as the integrated yields were also calculated for the reported spectra, which are furthermore added to Tab. 6. The inelastic pp cross section at $\sqrt{s} = 2.76$ TeV, quoted in [9] as well, was used to calculate the integrated yields which include extrapolation fractions of about 59% for the π^0 and about 52% for the η meson. The obtained values for $\langle p_T \rangle$ and $\mathrm{d}N/\mathrm{d}y$ for the neutral mesons were compared with measurements of average transverse momenta of charged particles [57] and with results concerning charged-particle multiplicity [58]. Due to a large extrapolation fraction of the π^0 and η spectra with respect to charged particles and the given systematics for the lowest transverse momenta, the uncertainties of $\langle p_T \rangle$ and $\mathrm{d}N/\mathrm{d}y$ are found to be larger. Hence, the integrated η/π^0 ratios are also affected. Nevertheless, all values quoted in this paragraph are consistent within uncertainties with the results from charged particle measurements. Within their substantial uncertainties, the η/π^0 ratios at both pp energies are found to be consistent as well.

$\sqrt{s} = 8$ TeV	$\langle p_T \rangle$ (GeV/c)	$\mathrm{d}N/\mathrm{d}y$	F_{extpol}
π^0	$0.426 \pm 0.006_{(\mathrm{stat})} \pm 0.023_{(\mathrm{sys})} \pm 0.018_{(\mathrm{fit\ sys})}$	$3.291 \pm 0.129_{(\mathrm{stat})} \pm 0.997_{(\mathrm{sys})} \pm 0.145_{(\mathrm{fit\ sys})}$	46%
η	$0.931 \pm 0.106_{(\mathrm{stat})} \pm 0.127_{(\mathrm{sys})} \pm 0.084_{(\mathrm{fit\ sys})}$	$0.163 \pm 0.032_{(\mathrm{stat})} \pm 0.053_{(\mathrm{sys})} \pm 0.024_{(\mathrm{fit\ sys})}$	33%
η/π^0	$0.050 \pm 0.010_{(\mathrm{stat})} \pm 0.022_{(\mathrm{sys})} \pm 0.008_{(\mathrm{fit\ sys})}$		

$\sqrt{s} = 2.76$ TeV	$\langle p_T \rangle$ (GeV/c)	$\mathrm{d}N/\mathrm{d}y$	F_{extpol}
π^0	$0.451 \pm 0.008_{(\mathrm{stat})} \pm 0.014_{(\mathrm{sys})} \pm 0.152_{(\mathrm{fit\ sys})}$	$1.803 \pm 0.058_{(\mathrm{stat})} \pm 0.352_{(\mathrm{sys})} \pm 0.646_{(\mathrm{fit\ sys})}$	59%
η	$0.647 \pm 0.068_{(\mathrm{stat})} \pm 0.040_{(\mathrm{sys})} \pm 0.140_{(\mathrm{fit\ sys})}$	$0.250 \pm 0.050_{(\mathrm{stat})} \pm 0.052_{(\mathrm{sys})} \pm 0.063_{(\mathrm{fit\ sys})}$	52%
η/π^0	$0.139 \pm 0.028_{(\mathrm{stat})} \pm 0.040_{(\mathrm{sys})} \pm 0.061_{(\mathrm{fit\ sys})}$		

Table 6: The mean transverse momenta, $\langle p_T \rangle$, and integrated yields, $\mathrm{d}N/\mathrm{d}y$, for ALICE measurements of π^0 and η mesons at $\sqrt{s} = 2.76$ and 8 TeV are summarized. It has to be noted that the uncertainties from the measurements of the inelastic cross sections are not included for the given numbers, which are $^{+3.9\%}_{-6.4\%}(model) \pm 2.0(lumi)\%$ for $\sqrt{s} = 2.76$ TeV [27] and $\pm 2.3\%$ for 8 TeV [56]. Moreover, the integrated η/π^0 ratios are quoted for the different energies.

Both meson spectra, which are shown in Fig. 7, exhibit a similar power-law behavior $E\mathrm{d}^3\sigma/\mathrm{d}p^3 \propto p_T^{-n}$ with $n_{\pi^0} = 5.939 \pm 0.013(\mathrm{stat}) \pm 0.025(\mathrm{sys})$ and $n_\eta = 5.931 \pm 0.029(\mathrm{stat}) \pm 0.046(\mathrm{sys})$ for $p_T > 3.5$ GeV/c. This is also reflected in the η/π^0 ratio which is shown in Fig. 8. The ratio is flat for $p_T > 3.5$ GeV/c with a constant value of $C^{\eta/\pi^0} = 0.455 \pm 0.006(\mathrm{stat}) \pm 0.014(\mathrm{sys})$. Despite of the inability of NLO calculations to describe individual π^0 and η meson spectra, the η/π^0 ratio is reproduced fairly well, as can be seen from left part of Fig. 8. It has to be noted that a different FF for the π^0 has been used to compile the theory curve, namely DSS07, since there was no recent η calculation available which could be compared to the recent DSS14 π^0 prediction. The agreement of pQCD calculations with the data can be viewed as an indication that the η/π^0 ratio is driven by the π^0 and η meson FFs in the factorized picture of pQCD. A comparison of the reported η/π^0 ratio to the different PYTHIA tunes indicates an agreement within uncertainties down to $p_{\mathrm{T}} \approx 1.5$ GeV$/c$, although the shape, as well as the ratio, cannot be fully reproduced below $p_{\mathrm{T}} < 1.5$ GeV$/c$ due to already mentioned deviations of PYTHIA tunes from data in this region.

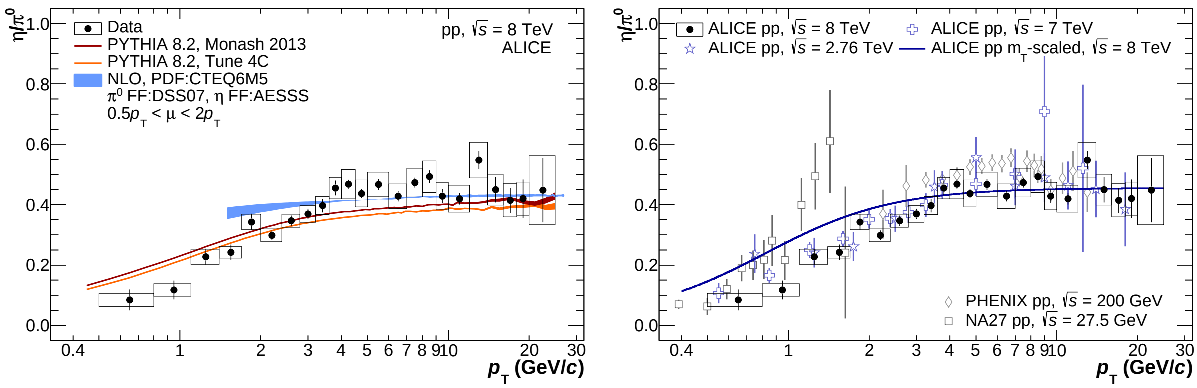

Fig. 8: Left: η/π^0 ratio compared to a NLO pQCD prediction, using PDF CTEQ6M5 and FFs DSS07 for the π^0 and AESSS for the η, and PYTHIA8.210 calculations using Tune 4C and Monash 2013 tune. Right: Comparison of the η/π^0 ratio to related, previous ALICE measurements as well as other experiments at lower collision energies, for which total uncertainties are drawn. Furthermore, a comparison to the η/π^0 ratio obtained with m_{T} scaling is added.

The validity of m_{T} scaling was tested by comparing the measured η/π^0 ratio with the ratio of the η spectrum, derived from the m_{T}-scaled TCM parametrization of the π^0 spectrum, to the fit of the measured π^0 spectrum. The quoted π^0 fit parameters from Tab. 5 were used as input for m_{T} scaling, further replacing the π^0 mass by the η mass and using the normalization ratio $C^{\eta}/C^{\pi^0} = 0.455$. The blue curve shown in the right plot of Fig. 8 displays the ratio of the m_{T}-scaled η spectrum to the fit of the π^0 spectrum. The measured η/π^0 ratio is consistent with the m_{T} scaling prediction above $p_{\mathrm{T}} > 3.5$ GeV$/c$. However, for smaller transverse momenta of $p_{\mathrm{T}} < 3.5$ GeV$/c$, the ratio of the measured η/π^0 ratio over the η/π^0 ratio obtained with m_{T} scaling constantly decreases and reaches about 45% at around 1 GeV$/c$. For the region below 3.5 GeV$/c$, m_{T} scaling is observed to be clearly broken with a significance of 6.2σ. Given this observation, the measured η/π^0 ratios in pp collisions at $\sqrt{s} = 2.76$ TeV and 7 TeV, which have previously been reported by ALICE [3, 9], were re-evaluated. Whereas there is indication for a m_{T} scaling violation with 2.1σ for 2.76 TeV, we also observe a significant disagreement of 5.7σ for 7 TeV. Hence, both ratios were found to be consistent with our observation at 8 TeV. Furthermore, both η/π^0 ratios were fitted with a constant for $p_{\mathrm{T}} > 3.5$ GeV$/c$, yielding values of $C^{\eta/\pi^0} = 0.474 \pm 0.015(\mathrm{stat}) \pm 0.024(\mathrm{sys})$ for 2.76 TeV and $C^{\eta/\pi^0} = 0.476 \pm 0.020(\mathrm{stat}) \pm 0.020(\mathrm{sys})$ for 7 TeV. They are consistent within uncertainties with the measured η/π^0 ratio at 8 TeV for the given p_{T} range. Therefore, all three ALICE measurements were simultaneously fitted with a constant for $p_{\mathrm{T}} > 3.5$ GeV$/c$ in order to obtain a combined value of $C^{\eta/\pi^0} = 0.459 \pm 0.006(\mathrm{stat}) \pm 0.011(\mathrm{sys})$. For the region $p_{\mathrm{T}} < 3.5$ GeV$/c$, all collision energies covered by ALICE also agree within experimental uncertainties, so that η/π^0 ratios may be claimed to be consistent within accuracy for ALICE measurements in pp collisions at $\sqrt{s} = 2.76$, 7 and 8 TeV.

Before the LHC era, the precision of η/π^0 measurements was not sufficient to probe m_{T} scaling over broad ranges of p_{T} with high statistics. PHENIX and NA27 measured the η/π^0 ratio with highest accuracy at high and low p_{T} and therefore are compared to the reported measurement. PHENIX measurements for pp collisions at $\sqrt{s} = 200$ GeV are available only for p_{T} region > 2.25 GeV$/c$ [59], where π^0 and η spectra are already described by m_{T} scaling. However, PHENIX has notably not applied any secondary π^0 correction concerning weak decays, which further has to be taken into account when comparing with data points from ALICE. Measurements of π^0 and η spectra in pp collisions at $\sqrt{s} = 27.5$ GeV from NA27 [60] were used to obtain the η/π^0 ratio in the p_{T} range of $0.4 < p_{\mathrm{T}} < 1.6$ GeV$/c$. The paper does not mention a secondary correction of neutral pion spectrum; however, it cannot significantly change the conclusions to be drawn from the measurement. Although the NA27 measurement provides the world's most precise published data points for the η/π^0 ratio at low $p_{\mathrm{T}} < 2.0$ GeV$/c$ in the pre-LHC era for pp collisions, it is not conclusive concerning m_{T} scaling violation. The first NA27 points at $p_{\mathrm{T}} < 1$ GeV$/c$ are consistent with both the m_{T} scaling curve and the new data from pp collisions at $\sqrt{s} = 2.76$, 7 and 8 TeV within uncertainties, whereas for $p_{\mathrm{T}} > 1$ GeV$/c$ the results of NA27 show a tendency to be above the m_{T} scaling prediction although uncertainties become significant. A clearer confirmation of the m_{T} scaling at low p_{T} was observed for other particle species, such as kaons, ϕ and J/ψ in pp collisions at $\sqrt{s} = 200$ GeV [11]. Whether the magnitude of m_{T} scaling violation depends on the collision energy can be clarified in future by ongoing analysis of hadron spectra measurements in pp collisions at $\sqrt{s} = 13$ TeV delivered by the LHC.

7 Conclusion

The invariant differential cross sections for inclusive π^0 and η meson production in pp collisions at $\sqrt{s}$ = 8 TeV have been measured at mid-rapidity over a wide p_{T} range by the ALICE experiment, using four different reconstruction methods for neutral pions, and three for η mesons. NLO pQCD calculations with MSTW08 PDF plus DSS14 FF for π^0 and CTEQ6M5 PDF plus AESSS FF for η mesons overestimate the measured spectra of both neutral mesons. This discrepancy has also been reported for pp collisions at $\sqrt{s} = 2.76$ TeV by ALICE. However, the ratio of η/π^0 is reproduced by NLO pQCD calculations within uncertainties, which is a test for the FFs in the factorized picture of pQCD. The prediction from PYTHIA8.2 Tune 4C describes the η spectrum within uncertainties for $p_{\mathrm{T}} > 1.5$ GeV$/c$, but it is about 30% larger than the measured π^0 production cross section. On the other hand, the Monash 2013 tune agrees with the reported neutral meson measurements within 10% for $p_{\mathrm{T}} > 1.5$ GeV$/c$. Both PYTHIA8.2 tunes are able to reproduce the π^0 spectrum below $p_{\mathrm{T}} < 1.5$ GeV$/c$ within uncertainties, but fail to describe the η spectrum in that region. The η/π^0 ratio is described by m_{T} scaling for $p_{\mathrm{T}} > 3.5$ GeV$/c$. For lower transverse momenta of $p_{\mathrm{T}} < 3.5$ GeV$/c$, the measurement deviates from this empirical scaling law with a significance of 6.2σ. Within experimental uncertainties, the η/π^0 ratios measured by NA27, PHENIX and ALICE are in agreement for the covered transverse momentum intervals of each measurement, representing pp collisions starting at center of mass energies of $\sqrt{s} = 27.5$ GeV up to $\sqrt{s} = 8$ TeV.

Acknowledgements

The ALICE Collaboration would like to thank all its engineers and technicians for their invaluable contributions to the construction of the experiment and the CERN accelerator teams for the outstanding performance of the LHC complex. The ALICE Collaboration gratefully acknowledges the resources and support provided by all Grid centres and the Worldwide LHC Computing Grid (WLCG) collaboration. The ALICE Collaboration acknowledges the following funding agencies for their support in building and running the ALICE detector: A. I. Alikhanyan National Science Laboratory (Yerevan Physics Institute) Foundation (ANSL), State Committee of Science and World Federation of Scientists (WFS), Armenia; Austrian Academy of Sciences and Nationalstiftung für Forschung, Technologie und Entwicklung, Austria; Ministry of Communications and High Technologies, National Nuclear Research Center, Azerbaijan; Conselho Nacional de Desenvolvimento Científico e Tecnológico (CNPq), Universidade Federal do Rio Grande do Sul (UFRGS), Financiadora de Estudos e Projetos (Finep) and Fundação de Amparo à Pesquisa do Estado de São Paulo (FAPESP), Brazil; Ministry of Science & Technology of China (MSTC), National Natural Science Foundation of China (NSFC) and Ministry of Education of China (MOEC) , China; Ministry of Science, Education and Sport and Croatian Science Foundation, Croatia;

Ministry of Education, Youth and Sports of the Czech Republic, Czech Republic; The Danish Council for Independent Research — Natural Sciences, the Carlsberg Foundation and Danish National Research Foundation (DNRF), Denmark; Helsinki Institute of Physics (HIP), Finland; Commissariat à l'Energie Atomique (CEA) and Institut National de Physique Nucléaire et de Physique des Particules (IN2P3) and Centre National de la Recherche Scientifique (CNRS), France; Bundesministerium für Bildung, Wissenschaft, Forschung und Technologie (BMBF) and GSI Helmholtzzentrum für Schwerionenforschung GmbH, Germany; General Secretariat for Research and Technology, Ministry of Education, Research and Religions, Greece; National Research, Development and Innovation Office, Hungary; Department of Atomic Energy Government of India (DAE) and Council of Scientific and Industrial Research (CSIR), New Delhi, India; Indonesian Institute of Science, Indonesia; Centro Fermi - Museo Storico della Fisica e Centro Studi e Ricerche Enrico Fermi and Istituto Nazionale di Fisica Nucleare (INFN), Italy; Institute for Innovative Science and Technology , Nagasaki Institute of Applied Science (IIST), Japan Society for the Promotion of Science (JSPS) KAKENHI and Japanese Ministry of Education, Culture, Sports, Science and Technology (MEXT), Japan; Consejo Nacional de Ciencia (CONACYT) y Tecnología, through Fondo de Cooperación Internacional en Ciencia y Tecnología (FONCICYT) and Dirección General de Asuntos del Personal Academico (DGAPA), Mexico; Nederlandse Organisatie voor Wetenschappelijk Onderzoek (NWO), Netherlands; The Research Council of Norway, Norway; Commission on Science and Technology for Sustainable Development in the South (COMSATS), Pakistan; Pontificia Universidad Católica del Perú, Peru; Ministry of Science and Higher Education and National Science Centre, Poland; Korea Institute of Science and Technology Information and National Research Foundation of Korea (NRF), Republic of Korea; Ministry of Education and Scientific Research, Institute of Atomic Physics and Romanian National Agency for Science, Technology and Innovation, Romania; Joint Institute for Nuclear Research (JINR), Ministry of Education and Science of the Russian Federation and National Research Centre Kurchatov Institute, Russia; Ministry of Education, Science, Research and Sport of the Slovak Republic, Slovakia; National Research Foundation of South Africa, South Africa; Centro de Aplicaciones Tecnológicas y Desarrollo Nuclear (CEADEN), Cubaenergía, Cuba, Ministerio de Ciencia e Innovacion and Centro de Investigaciones Energéticas, Medioambientales y Tecnológicas (CIEMAT), Spain; Swedish Research Council (VR) and Knut & Alice Wallenberg Foundation (KAW), Sweden; European Organization for Nuclear Research, Switzerland; National Science and Technology Development Agency (NSDTA), Suranaree University of Technology (SUT) and Office of the Higher Education Commission under NRU project of Thailand, Thailand; Turkish Atomic Energy Agency (TAEK), Turkey; National Academy of Sciences of Ukraine, Ukraine; Science and Technology Facilities Council (STFC), United Kingdom; National Science Foundation of the United States of America (NSF) and United States Department of Energy, Office of Nuclear Physics (DOE NP), United States of America.

References

[1] D. J. Gross and F. Wilczek, "Asymptotically Free Gauge Theories. 1," *Phys. Rev.* **D8** (1973) 3633–3652.

[2] L. Evans and P. Bryant, "LHC Machine," *JINST* **3** (2008) S08001.

[3] **ALICE** Collaboration, B. Abelev *et al.*, "Neutral pion and η meson production in proton-proton collisions at $\sqrt{s} = 0.9$ TeV and $\sqrt{s} = 7$ TeV," *Phys. Lett.* **B717** (2012) 162–172, arXiv:1205.5724 [hep-ex].

[4] **ALICE** Collaboration, B. B. Abelev *et al.*, "Neutral pion production at midrapidity in pp and Pb-Pb collisions at $\sqrt{s}$= 2.76 TeV," *Eur. Phys. J.* **C74** no. 10, (2014) 3108, arXiv:1405.3794 [nucl-ex].

[5] D. d'Enterria, K. J. Eskola, I. Helenius, and H. Paukkunen, "Confronting current NLO parton

fragmentation functions with inclusive charged-particle spectra at hadron colliders," *Nucl. Phys.* **B883** (2014) 615–628, arXiv:1311.1415 [hep-ph].

[6] D. de Florian, R. Sassot, and M. Stratmann, "Global analysis of fragmentation functions for pions and kaons and their uncertainties," *Phys. Rev.* **D75** (2007) 114010, arXiv:hep-ph/0703242 [hep-ph].

[7] D. de Florian, R. Sassot, and M. Stratmann, "Global analysis of fragmentation functions for protons and charged hadrons," *Phys. Rev.* **D76** (2007) 074033, arXiv:0707.1506 [hep-ph].

[8] D. de Florian, R. Sassot, M. Epele, R. J. Hernández-Pinto, and M. Stratmann, "Parton-to-Pion Fragmentation Reloaded," *Phys. Rev.* **D91** no. 1, (2015) 014035, arXiv:1410.6027 [hep-ph].

[9] **ALICE** Collaboration, S. Acharya *et al.*, "Production of π^0 and η mesons up to high transverse momentum in pp collisions at 2.76 TeV," arXiv:1702.00917 [hep-ex].

[10] D. d'Enterria, K. J. Eskola, I. Helenius, and H. Paukkunen, "LHC data challenges the contemporary parton-to-hadron fragmentation functions," *PoS* **DIS2014** (2014) 148, arXiv:1408.4659 [hep-ph].

[11] P. K. Khandai, P. Shukla, and V. Singh, "Meson spectra and m_T scaling in $p+p$, d+Au, and Au + Au collisions at $\sqrt{s_{NN}} = 200$ GeV," *Phys. Rev.* **C84** (2011) 054904, arXiv:1110.3929 [hep-ph].

[12] K. Jiang, Y. Zhu, W. Liu, H. Chen, C. Li, L. Ruan, Z. Tang, Z. Xu, and Z. Xu, "Onset of radial flow in p+p collisions," *Phys. Rev.* **C91** no. 2, (2015) 024910, arXiv:1312.4230 [nucl-ex].

[13] A. D. Martin, W. J. Stirling, R. S. Thorne, and G. Watt, "Parton distributions for the LHC," *Eur. Phys. J.* **C63** (2009) 189–285, arXiv:0901.0002 [hep-ph].

[14] W.K. Tung and H.L. Lai and A. Belyaev and J. Pumplin and D. Stump and C.-P. Yuan, "Heavy quark mass effects in deep inelastic scattering and global QCD analysis," *Journal of High Energy Physics* **2007** no. 02, (2007) 053. http://stacks.iop.org/1126-6708/2007/i=02/a=053.

[15] C. A. Aidala, F. Ellinghaus, R. Sassot, J. P. Seele, and M. Stratmann, "Global Analysis of Fragmentation Functions for Eta Mesons," *Phys. Rev.* **D83** (2011) 034002, arXiv:1009.6145 [hep-ph].

[16] T. Sjöstrand, S. Ask, J. R. Christiansen, R. Corke, N. Desai, P. Ilten, S. Mrenna, S. Prestel, C. O. Rasmussen, and P. Z. Skands, "An Introduction to PYTHIA 8.2," *Comput. Phys. Commun.* **191** (2015) 159–177, arXiv:1410.3012 [hep-ph].

[17] R. Corke and T. Sjöstrand, "Interleaved Parton Showers and Tuning Prospects," *JHEP* **03** (2011) 032, arXiv:1011.1759 [hep-ph].

[18] P. Skands, S. Carrazza, and J. Rojo, "Tuning PYTHIA 8.1: the Monash 2013 Tune," *Eur. Phys. J.* **C74** no. 8, (2014) 3024, arXiv:1404.5630 [hep-ph].

[19] **ALICE** Collaboration, K. Aamodt *et al.*, "The ALICE experiment at the CERN LHC," *JINST* **3** (2008) S08002.

[20] **ALICE** Collaboration, B. B. Abelev *et al.*, "Performance of the ALICE Experiment at the CERN LHC," *Int. J. Mod. Phys.* **A29** (2014) 1430044, arXiv:1402.4476 [nucl-ex].

[21] **ALICE** Collaboration, P. Cortese *et al.*, "ALICE electromagnetic calorimeter technical design report," CERN-LHCC-2008-014, CERN-ALICE-TDR-014.

[22] **ALICE** Collaboration, G. Dellacasa *et al.*, "ALICE technical design report of the photon spectrometer (PHOS)," CERN-LHCC-99-04.

[23] **ALICE** Collaboration, K. Aamodt *et al.*, "Alignment of the ALICE Inner Tracking System with cosmic-ray tracks," *JINST* **5** (2010) P03003, `arXiv:1001.0502 [physics.ins-det]`.

[24] J. Alme *et al.*, "The ALICE TPC, a large 3-dimensional tracking device with fast readout for ultra-high multiplicity events," *Nucl. Instrum. Meth.* **A622** (2010) 316–367, `arXiv:1001.1950 [physics.ins-det]`.

[25] **ALICE EMCal** Collaboration, U. Abeysekara *et al.*, "ALICE EMCal Physics Performance Report," `arXiv:1008.0413 [physics.ins-det]`.

[26] **ALICE** Collaboration, P. Cortese *et al.*, "ALICE technical design report on forward detectors: FMD, T0 and V0," CERN-LHCC-2004-025.

[27] **ALICE** Collaboration, B. Abelev *et al.*, "Measurement of inelastic, single- and double-diffraction cross sections in proton–proton collisions at the LHC with ALICE," *Eur. Phys. J.* **C73** no. 6, (2013) 2456, `arXiv:1208.4968 [hep-ex]`.

[28] J. Kral, T. Awes, H. Muller, J. Rak, and J. Schambach, "L0 trigger for the EMCal detector of the ALICE experiment," *Nucl. Instrum. Meth.* **A693** (2012) 261–267.

[29] D. Wang *et al.*, "Level-0 trigger algorithms for the ALICE PHOS detector," *Nucl. Instrum. Meth.* **A629** (2011) 80–86.

[30] J. Adam *et al.*, "Determination of the event collision time with the ALICE detector at the LHC," *The European Physical Journal Plus* **132** no. 2, (Feb, 2017) 99. `https://doi.org/10.1140/epjp/i2017-11279-1`.

[31] S. van der Meer, "Calibration of the Effective Beam Height in the ISR." CERN-ISR-PO-68-31, 1968.

[32] **ALICE** Collaboration, S. Acharya *et al.*, "ALICE luminosity determination for pp collisions at $\sqrt{s} = 8$ TeV,". `https://cds.cern.ch/record/2255216`.

[33] **Particle Data Group** Collaboration, C. Patrignani *et al.*, "Review of Particle Physics," *Chin. Phys.* **C40** no. 10, (2016) 100001.

[34] **ALICE** Collaboration, P. Cortese *et al.*, "ALICE: Physics performance report, volume II," *J. Phys.* **G32** (2006) 1295–2040.

[35] T. Awes, F. Obenshain, F. Plasil, S. Saini, S. Sorensen, and G. Young, "A simple method of shower localization and identification in laterally segmented calorimeters," *Nuclear Instruments and Methods in Physics Research Section A: Accelerators, Spectrometers, Detectors and Asso* `http://www.sciencedirect.com/science/article/pii/0168900292908582`.

[36] S. Gorbunov and I. Kisel, "Reconstruction of decayed particles based on the Kalman filter," *CBM-SOFT-note* **003** (2007) 1–16. `http://web-docs.gsi.de/~ikisel/reco/CBM/DOC-2007-May-14-1.pdf`.

[37] J. Podolanski and R. Armenteros, "III. Analysis of V-events," *Phil. Mag.* **45** no. 360, (1954) 13–30.

[38] G. Kopylov, "Like particle correlations as a tool to study the multiple production mechanism," *Physics Letters B* **50** no. 4, (1974) 472 – 474. `http://www.sciencedirect.com/science/article/pii/0370269374902639`.

[39] M. J. Oreglia, *A Study of the Reactions $\psi\prime \rightarrow \gamma\gamma\psi$*. PhD thesis, SLAC, Stanford University, Stanford, California 94305, 1980. http://www.slac.stanford.edu/pubs/slacreports/slac-r-236.html.

[40] T. Matulewicz *et al.* , "Response of BaF2 detectors to photons of 3-50 MeV energy," *Nuclear Instruments and Methods in Physics Research Section A: Accelerators, Spectrometers, Detectors and Ass*

[41] R. Brun, F. Bruyant, M. Maire, A. McPherson, and P. Zanarini, "GEANT3." CERN-DD-EE-84-1, 1987.

[42] R. Engel, J. Ranft, and S. Roesler, "Hard diffraction in hadron hadron interactions and in photoproduction," *Phys. Rev.* **D52** (1995) 1459–1468, arXiv:hep-ph/9502319 [hep-ph].

[43] **ALICE** Collaboration, K. Aamodt *et al.*, "Strange particle production in proton-proton collisions at sqrt(s) = 0.9 TeV with ALICE at the LHC," *Eur. Phys. J.* **C71** (2011) 1594, arXiv:1012.3257 [hep-ex].

[44] **ALICE** Collaboration, B. B. Abelev *et al.*, "Production of charged pions, kaons and protons at large transverse momenta in pp and Pb–Pb collisions at $\sqrt{s_{\rm NN}}$ =2.76 TeV," *Phys. Lett.* **B736** (2014) 196–207, arXiv:1401.1250 [nucl-ex].

[45] **ALICE** Collaboration, J. Adam *et al.*, "Multiplicity-dependent enhancement of strange and multi-strange hadron production in proton-proton collisions at $\sqrt{s} = 7$ TeV," arXiv:1606.07424 [nucl-ex].

[46] L. Lyons, D. Gibaut, and P. Clifford, "How to Combine Correlated Estimates of a Single Physical Quantity," *Nucl.Instrum.Meth.* **A270** (1988) 110.

[47] A. Valassi, "Combining correlated measurements of several different physical quantities," *Nucl.Instrum.Meth.* **A500** (2003) 391–405.

[48] L. Lyons, *Statistics For Nuclear And Particle Physicists*. Cambridge, UK: Univ. Pr., 1986.

[49] R. J. Barlow, *Statistics: a guide to the use of statistical methods in the physical sciences*, vol. 29. John Wiley & Sons, 1989.

[50] A. Valassi and R. Chierici, "Information and treatment of unknown correlations in the combination of measurements using the BLUE method," *Eur.Phys.J.* **C74** (2014) 2717, arXiv:1307.4003 [physics.data-an].

[51] G. Lafferty and T. Wyatt, "Where to stick your data points: The treatment of measurements within wide bins," *Nucl. Instrum. Meth.* **A355** no. 2, (1995) 541–547.

[52] A. Bylinkin, N. S. Chernyavskaya, and A. A. Rostovtsev, "Predictions on the transverse momentum spectra for charged particle production at LHC-energies from a two component model," *Eur. Phys. J.* **C75** no. 4, (2015) 166, arXiv:1501.05235 [hep-ph].

[53] C. Tsallis, "Possible Generalization of Boltzmann-Gibbs Statistics," *J.Statist.Phys.* **52** (1988) 479–487.

[54] **PHENIX** Collaboration, A. Adare *et al.*, "Inclusive cross section and double-helicity asymmetry for π^0 production at midrapidity in p+p collisions at $\sqrt{s} = 510$ GeV," *Phys. Rev.* **D93** no. 1, (2016) 011501, arXiv:1510.02317 [hep-ex].

[55] **PHENIX** Collaboration, A. Adare *et al.*, "Detailed measurement of the e^+e^- pair continuum in $p+p$ and Au + Au collisions at $\sqrt{s_{NN}} = 200$ GeV and implications for direct photon production," *Phys. Rev. C* **81** (Mar, 2010) 034911.
https://link.aps.org/doi/10.1103/PhysRevC.81.034911.

[56] **TOTEM** Collaboration, G. Antchev *et al.*, "Luminosity-independent measurement of the proton-proton total cross section at $\sqrt{s} = 8$ TeV," *Phys. Rev. Lett.* **111** (Jul, 2013) 012001.
https://link.aps.org/doi/10.1103/PhysRevLett.111.012001.

[57] **ALICE** Collaboration, B. B. Abelev *et al.*, "Multiplicity dependence of the average transverse momentum in pp, p-Pb, and Pb-Pb collisions at the LHC," *Phys. Lett.* **B727** (2013) 371–380, arXiv:1307.1094 [nucl-ex].

[58] **ALICE** Collaboration, J. Adam *et al.*, "Charged-particle multiplicities in proton–proton collisions at $\sqrt{s} = 0.9$ to 8 TeV," *Eur. Phys. J.* **C77** no. 1, (2017) 33, arXiv:1509.07541 [nucl-ex].

[59] **PHENIX** Collaboration, A. Adare *et al.*, "Cross section and double helicity asymmetry for eta mesons and their comparison to neutral pion production in p+p collisions at sqrt(s)=200 GeV," *Phys. Rev.* **D83** (2011) 032001, arXiv:1009.6224 [hep-ex].

[60] **LEBC-EHS** Collaboration, M. Aguilar-Benitez *et al.*, "Inclusive particle production in 400 GeV/c pp-interactions," *Z. Phys.* **C50** (1991) 405–426.

A The ALICE Collaboration

S. Acharya[137] , , J. Adam[96] , , D. Adamová[93] , , J. Adolfsson[32] , , M.M. Aggarwal[98] , , G. Aglieri Rinella[33] , , M. Agnello[29] , , N. Agrawal[46] , , Z. Ahammed[137] , , N. Ahmad[15] , , S.U. Ahn[78] , , S. Aiola[141] , , A. Akindinov[63] , , M. Al-Turany[106] , , S.N. Alam[137] , , J.L.B. Alba[111] , , D.S.D. Albuquerque[122] , , D. Aleksandrov[89] , , B. Alessandro[57] , , R. Alfaro Molina[73] , , A. Alici[11 ,25 ,52] , , A. Alkin[3] , , J. Alme[20] , , T. Alt[69] , , L. Altenkamper[20] , , I. Altsybeev[136] , , C. Alves Garcia Prado[121] , , C. Andrei[86] , , D. Andreou[33] , , H.A. Andrews[110] , , A. Andronic[106] , , V. Anguelov[103] , , C. Anson[96] , , T. Antičić[107] , , F. Antinori[55] , , P. Antonioli[52] , , R. Anwar[124] , , L. Aphecetche[114] , , H. Appelshäuser[69] , , S. Arcelli[25] , , R. Arnaldi[57] , , O.W. Arnold[104 ,34] , , I.C. Arsene[19] , , M. Arslandok[103] , , B. Audurier[114] , , A. Augustinus[33] , , R. Averbeck[106] , , M.D. Azmi[15] , , A. Badalà[54] , , Y.W. Baek[59 ,77] , , S. Bagnasco[57] , , R. Bailhache[69] , , R. Bala[100] , , A. Baldisseri[74] , , M. Ball[43] , , R.C. Baral[66 ,87] , , A.M. Barbano[24] , , R. Barbera[26] , , F. Barile[51 ,31] , , L. Barioglio[24] , , G.G. Barnaföldi[140] , , L.S. Barnby[92] , , V. Barret[131] , , P. Bartalini[7] , , K. Barth[33] , , E. Bartsch[69] , , M. Basile[25] , , N. Bastid[131] , , S. Basu[139] , , G. Batigne[114] , , B. Batyunya[76] , , P.C. Batzing[19] , , I.G. Bearden[90] , , H. Beck[103] , , C. Bedda[62] , , N.K. Behera[59] , , I. Belikov[133] , , F. Bellini[25 ,33] , , H. Bello Martinez[2] , , R. Bellwied[124] , , L.G.E. Beltran[120] , , V. Belyaev[82] , , G. Bencedi[140] , , S. Beole[24] , , A. Bercuci[86] , , Y. Berdnikov[95] , , D. Berenyi[140] , , R.A. Bertens[127] , , D. Berzano[33] , , L. Betev[33] , , A. Bhasin[100] , , I.R. Bhat[100] , , A.K. Bhati[98] , , B. Bhattacharjee[42] , , J. Bhom[118] , , A. Bianchi[24] , , L. Bianchi[124] , , N. Bianchi[49] , , C. Bianchin[139] , , J. Bielčík[37] , , J. Bielčíková[93] , , A. Bilandzic[34 ,104] , , G. Biro[140] , , R. Biswas[4] , , S. Biswas[4] , , J.T. Blair[119] , , D. Blau[89] , , C. Blume[69] , , G. Boca[134] , , F. Bock[103 ,81 ,33] , , A. Bogdanov[82] , , L. Boldizsár[140] , , M. Bombara[38] , , G. Bonomi[135] , , M. Bonora[33] , , J. Book[69] , , H. Borel[74] , , A. Borissov[17 ,103] , , M. Borri[126] , , E. Botta[24] , , C. Bourjau[90] , , L. Bratrud[69] , , P. Braun-Munzinger[106] , , M. Bregant[121] , , T.A. Broker[69] , , M. Broz[37] , , E.J. Brucken[44] , , E. Bruna[57] , , G.E. Bruno[33 ,31] , , D. Budnikov[108] , , H. Buesching[69] , , S. Bufalino[29] , , P. Buhler[113] , , P. Buncic[33] , , O. Busch[130] , , Z. Buthelezi[75] , , J.B. Butt[14] , , J.T. Buxton[16] , , J. Cabala[116] , , D. Caffarri[33 ,91] , , H. Caines[141] , , A. Caliva[62 ,106] , , E. Calvo Villar[111] , , P. Camerini[23] , , A.A. Capon[113] , , F. Carena[33] , , W. Carena[33] , , F. Carnesecchi[25 ,11] , , J. Castillo Castellanos[74] , , A.J. Castro[127] , , E.A.R. Casula[53] , , C. Ceballos Sanchez[9] , , P. Cerello[57] , , S. Chandra[137] , , B. Chang[125] , , S. Chapeland[33] , , M. Chartier[126] , , S. Chattopadhyay[137] , , S. Chattopadhyay[109] , , A. Chauvin[34 ,104] , , C. Cheshkov[132] , , B. Cheynis[132] , , V. Chibante Barroso[33] , , D.D. Chinellato[122] , , S. Cho[59] , , P. Chochula[33] , , M. Chojnacki[90] , , S. Choudhury[137] , , T. Chowdhury[131] , , P. Christakoglou[91] , , C.H. Christensen[90] , , P. Christiansen[32] , , T. Chujo[130] , , S.U. Chung[17] , , C. Cicalo[53] , , L. Cifarelli[11 ,25] , , F. Cindolo[52] , , J. Cleymans[99] , , F. Colamaria[31] , , D. Colella[33 ,64 ,51] , , A. Collu[81] , , M. Colocci[25] , , M. Concas[57 ,,ii] , , G. Conesa Balbastre[80] , , Z. Conesa del Valle[60] , , M.E. Connors[141 ,,iii] , , J.G. Contreras[37] , , T.M. Cormier[94] , , Y. Corrales Morales[57] , , I. Cortés Maldonado[2] , , P. Cortese[30] , , M.R. Cosentino[123] , , F. Costa[33] , , S. Costanza[134] , , J. Crkovská[60] , , P. Crochet[131] , , E. Cuautle[71] , , L. Cunqueiro[70] , , T. Dahms[34 ,104] , , A. Dainese[55] , , M.C. Danisch[103] , , A. Danu[67] , , D. Das[109] , , I. Das[109] , , S. Das[4] , , A. Dash[87] , , S. Dash[46] , , S. De[47 ,121] , , A. De Caro[28] , , G. de Cataldo[51] , , C. de Conti[121] , , J. de Cuveland[40] , , A. De Falco[22] , , D. De Gruttola[28 ,11] , , N. De Marco[57] , , S. De Pasquale[28] , , R.D. De Souza[122] , , H.F. Degenhardt[121] , , A. Deisting[106 ,103] , , A. Deloff[85] , , C. Deplano[91] , , P. Dhankher[46] , , D. Di Bari[31] , , A. Di Mauro[33] , , P. Di Nezza[49] , , B. Di Ruzza[55] , , T. Dietel[99] , , P. Dillenseger[69] , , R. Divià[33] , , Ø. Djuvsland[20] , , A. Dobrin[33] , , D. Domenicis Gimenez[121] , , B. Dönigus[69] , , O. Dordic[19] , , L.V.R. Doremalen[62] , , A.K. Dubey[137] , , A. Dubla[106] , , L. Ducroux[132] , , A.K. Duggal[98] , , M. Dukhishyam[87] , , P. Dupieux[131] , , R.J. Ehlers[141] , , D. Elia[51] , , E. Endress[111] , , H. Engel[68] , , E. Epple[141] , , B. Erazmus[114] , , F. Erhardt[97] , , B. Espagnon[60] , , S. Esumi[130] , , G. Eulisse[33] , , J. Eum[17] , , D. Evans[110] , , S. Evdokimov[112] , , L. Fabbietti[104 ,34] , , J. Faivre[80] , , A. Fantoni[49] , , M. Fasel[94 ,81] , , L. Feldkamp[70] , , A. Feliciello[57] , , G. Feofilov[136] , , A. Fernández Téllez[2] , , A. Ferretti[24] , , A. Festanti[27 ,33] , , V.J.G. Feuillard[74 ,131] , , J. Figiel[118] , , M.A.S. Figueredo[121] , , S. Filchagin[108] , , D. Finogeev[61] , , F.M. Fionda[20 ,22] , , M. Floris[33] , , S. Foertsch[75] , , P. Foka[106] , , S. Fokin[89] , , E. Fragiacomo[58] , , A. Francescon[33] , , A. Francisco[114] , , U. Frankenfeld[106] , , G.G. Fronze[24] , , U. Fuchs[33] , , C. Furget[80] , , A. Furs[61] , , M. Fusco Girard[28] , , J.J. Gaardhøje[90] , , M. Gagliardi[24] , , A.M. Gago[111] , , K. Gajdosova[90] , , M. Gallio[24] , , C.D. Galvan[120] , , P. Ganoti[84] , , C. Garabatos[106] , , E. Garcia-Solis[12] , , K. Garg[26] , , C. Gargiulo[33] , , P. Gasik[104 ,34] , , E.F. Gauger[119] , , M.B. Gay Ducati[72] , , M. Germain[114] , , J. Ghosh[109] , , P. Ghosh[137] , , S.K. Ghosh[4] , , P. Gianotti[49] , , P. Giubellino[33 ,106 ,57] , , P. Giubilato[27] , , E. Gladysz-Dziadus[118] , , P. Glässel[103] , , D.M. Goméz Coral[73] , , A. Gomez Ramirez[68] , , A.S. Gonzalez[33] , , P. González-Zamora[2] , , S. Gorbunov[40] , , L. Görlich[118] , , S. Gotovac[117] , , V. Grabski[73] , , L.K. Graczykowski[138] , , K.L. Graham[110] , , L. Greiner[81] , , A. Grelli[62] , , C. Grigoras[33] , , V. Grigoriev[82] , , A. Grigoryan[1] , , S. Grigoryan[76] , , J.M. Gronefeld[106] , , F. Grosa[29] , , J.F. Grosse-Oetringhaus[33] , , R. Grosso[106] , , L. Gruber[113] , , F. Guber[61] , , R. Guernane[80] , , B. Guerzoni[25] , , K. Gulbrandsen[90] , , T. Gunji[129] , , A. Gupta[100] , , R. Gupta[100] , , I.B. Guzman[2] , , R. Haake[33] , , C. Hadjidakis[60] , , H. Hamagaki[83] , , G. Hamar[140] , , J.C. Hamon[133] , , M.R. Haque[62] , , J.W. Harris[141] , , A. Harton[12] , , H. Hassan[80] , , D. Hatzifotiadou[11 ,52] , , S. Hayashi[129] , , S.T. Heckel[69] , , E. Hellbär[69] , , H. Helstrup[35] , , A. Herghelegiu[86] , , E.G. Hernandez[2] , , G. Herrera Corral[10] , , F. Herrmann[70] , , B.A. Hess[102] , , K.F. Hetland[35] , , H. Hillemanns[33] , , C. Hills[126] , , B. Hippolyte[133] , , J. Hladky[65] , , B. Hohlweger[104] , , D. Horak[37] , , S. Hornung[106] , , R. Hosokawa[130 ,80] , , P. Hristov[33] , , C. Hughes[127] , , T.J. Humanic[16] , , N. Hussain[42] , , T. Hussain[15] , , D. Hutter[40] , , D.S. Hwang[18] , , S.A. Iga Buitron[71] , , R. Ilkaev[108] , , M. Inaba[130] , , M. Ippolitov[82 ,89] , , M. Irfan[15] , , M.S. Islam[109] , , M. Ivanov[106] , , V. Ivanov[95] , , V. Izucheev[112] , , B. Jacak[81] , , N. Jacazio[25] , , P.M. Jacobs[81] , , M.B. Jadhav[46] , , J. Jadlovsky[116] , , S. Jaelani[62] , , C. Jahnke[34] , , M.J. Jakubowska[138] , , M.A. Janik[138] , , P.H.S.Y. Jayarathna[124] , , C. Jena[87] , , S. Jena[124] , , M. Jercic[97] , , R.T. Jimenez Bustamante[106] , , P.G. Jones[110] , , A. Jusko[110] , , P. Kalinak[64] , , A. Kalweit[33] , , J.H. Kang[142] , , V. Kaplin[82] , , S. Kar[137] , , A. Karasu Uysal[79] , , O. Karavichev[61] , , T. Karavicheva[61] , , L. Karayan[103 ,106] , , P. Karczmarczyk[33] , , E. Karpechev[61] , , U. Kebschull[68] , , R. Keidel[143] , , D.L.D. Keijdener[62] , , M. Keil[33] , , B. Ketzer[43] , , Z. Khabanova[91] , , P. Khan[109] , , S.A. Khan[137] , , A. Khanzadeev[95] , , Y. Kharlov[112] , , A. Khatun[15] , , A. Khuntia[47] , , M.M. Kielbowicz[118] , , B. Kileng[35] , , B. Kim[130] , , D. Kim[142] , , D.J. Kim[125] , , H. Kim[142] , , J.S. Kim[41] , , J. Kim[103] , , M. Kim[59] , , M. Kim[142] , , S. Kim[18] , , T. Kim[142] , , S. Kirsch[40] , , I. Kisel[40] , , S. Kiselev[63] , , A. Kisiel[138] , , G. Kiss[140] , , J.L. Klay[6] , , C. Klein[69] , , J. Klein[33] , , C. Klein-Bösing[70] , , S. Klewin[103] , , A. Kluge[33] , , M.L. Knichel[33 ,103] , , A.G. Knospe[124] , , C. Kobdaj[115] , , M. Kofarago[140] , , M.K. Köhler[103] , , T. Kollegger[106] , , V. Kondratiev[136] , , N. Kondratyeva[82] , , E. Kondratyuk[112] , , A. Konevskikh[61] , , M. Konyushikhin[139] , , M. Kopcik[116] , , M. Kour[100] , , C. Kouzinopoulos[33] , , O. Kovalenko[85] , , V. Kovalenko[136] , , M. Kowalski[118] , , G. Koyithatta Meethaleveedu[46] , , I. Králik[64] , , A. Kravčáková[38] , , L. Kreis[106] , , M. Krivda[110 ,64] , , F. Krizek[93] , , E. Kryshen[95] , , M. Krzewicki[40] , , A.M. Kubera[16] , , V. Kučera[93] , , C. Kuhn[133] , , P.G. Kuijer[91] , , A. Kumar[100] , , J. Kumar[46] , , L. Kumar[98] , , S. Kumar[46] , , S. Kundu[87] , , P. Kurashvili[85] , , A. Kurepin[61] , , A.B. Kurepin[61] , , A. Kuryakin[108] , , S. Kushpil[93] , , M.J. Kweon[59] , , Y. Kwon[142] , , S.L. La Pointe[40] , , P. La Rocca[26] , , C. Lagana Fernandes[121] , , Y.S. Lai[81] , , I. Lakomov[33] , , R. Langoy[39] , , K. Lapidus[141] , , C. Lara[68] , , A. Lardeux[74 ,19] , , A. Lattuca[24] , , E. Laudi[33] , , R. Lavicka[37] , , R. Lea[23] , , L. Leardini[103] , , S. Lee[142] , , F. Lehas[91] , , S. Lehner[113] , , J. Lehrbach[40] , , R.C. Lemmon[92] , , V. Lenti[51] , , E. Leogrande[62] , , I. León Monzón[120] , , P. Lévai[140] , , X. Li[13] , , J. Lien[39] , , R. Lietava[110] , , B. Lim[17] , , S. Lindal[19] , , V. Lindenstruth[40] , , S.W. Lindsay[126] , , C. Lippmann[106] , , M.A. Lisa[16] , , V. Litichevskyi[44] , , W.J. Llope[139] , , D.F. Lodato[62] , , P.I. Loenne[20] , , V. Loginov[82] , , C. Loizides[81] , , P. Loncar[117] , , X. Lopez[131] , , E. López Torres[9] , , A. Lowe[140] , , P. Luettig[69] , , J.R. Luhder[70] , , M. Lunardon[27] , , G. Luparello[58 ,23] , , M. Lupi[33] , , T.H. Lutz[141] , , A. Maevskaya[61] , , M. Mager[33] , , S. Mahajan[100] , , S.M. Mahmood[19] , , A. Maire[133] , , R.D. Majka[141] , , M. Malaev[95] , , L. Malinina[76 ,,iv] , , D. Mal'Kevich[63] , , P. Malzacher[106] , , A. Mamonov[108] , , V. Manko[89] , , F. Manso[131] , , V. Manzari[51] , , Y. Mao[7] , , M. Marchisone[75 ,128] , , J. Mareš[65] , , G.V. Margagliotti[23] , , A. Margotti[52] , , J. Margutti[62] , , A. Marín[106] , , C. Markert[119] , , M. Marquard[69] , , N.A. Martin[106] , , P. Martinengo[33] , , J.A.L. Martinez[68] , , M.I. Martínez[2] , , G. Martínez García[114] , , M. Martinez Pedreira[33] , , S. Masciocchi[106] , , M. Masera[24] , , A. Masoni[53] , , E. Masson[114] , , A. Mastroserio[51] , , A.M. Mathis[104 ,34] , , P.F.T. Matuoka[121] , , A. Matyja[127] , , C. Mayer[118] , , J. Mazer[127] , , M. Mazzilli[31] , , M.A. Mazzoni[56] , , F. Meddi[21] , , Y. Melikyan[82] , , A. Menchaca-Rocha[73] , , E. Meninno[28] , , J. Mercado Pérez[103] , , M. Meres[36] , , S. Mhlanga[99] , , Y. Miake[130] , , M.M. Mieskolainen[44] , , D.L. Mihaylov[104] , , K. Mikhaylov[63 ,76] , , J. Milosevic[19] , , A. Mischke[62] , , A.N. Mishra[47] , , D. Miśkowiec[106] , , J. Mitra[137] , , C.M. Mitu[67] , , N. Mohammadi[62] , , B. Mohanty[87] , , M. Mohisin Khan[15 ,,v] , , D.A. Moreira De Godoy[70] , , L.A.P. Moreno[2] , , S. Moretto[27] , , A. Morreale[114] , , A. Morsch[33] , , V. Muccifora[49] , , E. Mudnic[117] , , D. Mühlheim[70] , , S. Muhuri[137] , , M. Mukherjee[4] , , J.D. Mulligan[141] , , M.G. Munhoz[121] , , K. Münning[43] , , R.H. Munzer[69] , , H. Murakami[129] , , S. Murray[75] , , L. Musa[33] , , J. Musinsky[64] , , C.J. Myers[124] , , J.W. Myrcha[138] , , D. Nag[4] , , B. Naik[46] , , R. Nair[85] , , B.K. Nandi[46] , , R. Nania[52 ,11] , , E. Nappi[51] , , A. Narayan[46] , , M.U. Naru[14] , , H. Natal da Luz[121] , , C. Nattrass[127] , , S.R. Navarro[2] , , K. Nayak[87] , , R. Nayak[46] , , T.K. Nayak[137] , , S. Nazarenko[108] , , A. Nedosekin[63] , , R.A. Negrao De Oliveira[33] , , L. Nellen[71] , , S.V. Nesbo[35] , , F. Ng[124] , , M. Nicassio[106] , , M. Niculescu[67] , , J. Niedziela[138 ,33] , , B.S. Nielsen[90] , , S. Nikolaev[89] , , S. Nikulin[89] , , V. Nikulin[95] , , F. Noferini[11 ,52] , , P. Nomokonov[76] , , G. Nooren[62] , , J.C.C. Noris[2] , , J. Norman[126] , , A. Nyanin[89] , , J. Nystrand[20] , , H. Oeschler[17 ,103 ,,i] , , S. Oh[141] , , A. Ohlson[33 ,103] , , T. Okubo[45] , , L. Olah[140] , , J. Oleniacz[138] , , A.C. Oliveira Da Silva[121] , , M.H. Oliver[141] , , J. Onderwaater[106] , , C. Oppedisano[57] , , R. Orava[44] , , M. Oravec[116] , , A. Ortiz Velasquez[71] , , A. Oskarsson[32] , , J. Otwinowski[118] , , K. Oyama[83] , , Y. Pachmayer[103] , , V. Pacik[90] , , D. Pagano[135] , , P. Pagano[28] , , G. Paić[71] , , P. Palni[7] , , J. Pan[139] , , A.K. Pandey[46] , , S. Panebianco[74] , , V. Papikyan[1] , , G.S. Pappalardo[54] , , P. Pareek[47] , , J. Park[59] , , S. Parmar[98] , , A. Passfeld[70] , , S.P. Pathak[124] , , R.N. Patra[137] , , B. Paul[57] , , H. Pei[7] , , T. Peitzmann[62] , , X. Peng[7] , , L.G. Pereira[72] , , H. Pereira Da Costa[74] , , D. Peresunko[89 ,82] , , E. Perez Lezama[69] , , V. Peskov[69] , , Y. Pestov[5] , , V. Petráček[37] , , V. Petrov[112] , , M. Petrovici[86] , , C. Petta[26] , , R.P. Pezzi[72] , ,

S. Piano[58] , , M. Pikna[36] , , P. Pillot[114] , , L.O.D.L. Pimentel[90] , , O. Pinazza[52 ,33] , , L. Pinsky[124] , , D.B. Piyarathna[124] , , M. Płoskoń[81] , , M. Planinic[97] , , F. Pliquett[69] , , J. Pluta[138] , , S. Pochybova[140] , , P.L.M. Podesta-Lerma[120] , , M.G. Poghosyan[94] , , B. Polichtchouk[112] , , N. Poljak[97] , , W. Poonsawat[115] , , A. Pop[86] , , H. Poppenborg[70] , , S. Porteboeuf-Houssais[131] , , V. Pozdniakov[76] , , S.K. Prasad[4] , , R. Preghenella[52] , , F. Prino[57] , , C.A. Pruneau[139] , , I. Pshenichnov[61] , , M. Puccio[24] , , G. Puddu[22] , , P. Pujahari[139] , , V. Punin[108] , , J. Putschke[139] , , S. Raha[4] , , S. Rajput[100] , , J. Rak[125] , , A. Rakotozafindrabe[74] , , L. Ramello[30] , , F. Rami[133] , , D.B. Rana[124] , , R. Raniwala[101] , , S. Raniwala[101] , , S.S. Räsänen[44] , , B.T. Rascanu[69] , , D. Rathee[98] , , V. Ratza[43] , , I. Ravasenga[29] , , K.F. Read[127 ,94] , , K. Redlich[85 ,,vi] , A. Rehman[20] , , P. Reichelt[69] , , F. Reidt[33] , , X. Ren[7] , , R. Renfordt[69] , , A.R. Reolon[49] , , A. Reshetin[61] , , K. Reygers[103] , , V. Riabov[95] , , R.A. Ricci[50] , , T. Richert[32] , , M. Richter[19] , , P. Riedler[33] , , W. Riegler[33] , , F. Riggi[26] , , C. Ristea[67] , , M. Rodríguez Cahuantzi[2] , , K. Røed[19] , , E. Rogochaya[76] , , D. Rohr[33 ,40] , , D. Röhrich[20] , , P.S. Rokita[138] , , F. Ronchetti[49] , , E.D. Rosas[71] , , P. Rosnet[131] , , A. Rossi[27 ,55] , , A. Rotondi[134] , , F. Roukoutakis[84] , , A. Roy[47] , , C. Roy[133] , , P. Roy[109] , , O.V. Rueda[71] , , R. Rui[23] , , B. Rumyantsev[76] , , A. Rustamov[88] , , E. Ryabinkin[89] , , Y. Ryabov[95] , , A. Rybicki[118] , , S. Saarinen[44] , , S. Sadhu[137] , , S. Sadovsky[112] , , K. Šafařík[33] , , S.K. Saha[137] , , B. Sahlmuller[69] , , B. Sahoo[46] , , P. Sahoo[47] , , R. Sahoo[47] , , S. Sahoo[66] , , P.K. Sahu[66] , , J. Saini[137] , , S. Sakai[130] , , M.A. Saleh[139] , , J. Salzwedel[16] , , S. Sambyal[100] , , V. Samsonov[95 ,82] , , A. Sandoval[73] , , D. Sarkar[137] , , N. Sarkar[137] , , P. Sarma[42] , , M.H.P. Sas[62] , , E. Scapparone[52] , , F. Scarlassara[27] , , B. Schaefer[94] , , R.P. Scharenberg[105] , , H.S. Scheid[69] , , C. Schiaua[86] , , R. Schicker[103] , , C. Schmidt[106] , , H.R. Schmidt[102] , , M.O. Schmidt[103] , , M. Schmidt[102] , , N.V. Schmidt[94 ,69] , , J. Schukraft[33] , , Y. Schutz[33 ,133] , , K. Schwarz[106] , , K. Schweda[106] , , G. Scioli[25] , , E. Scomparin[57] , , M. Šefčík[38] , , J.E. Seger[96] , , Y. Sekiguchi[129] , , D. Sekihata[45] , , I. Selyuzhenkov[106 ,82] , , K. Senosi[75] , , S. Senyukov[3 ,133 ,33] , , E. Serradilla[73] , , P. Sett[46] , , A. Sevcenco[67] , , A. Shabanov[61] , , A. Shabetai[114] , , R. Shahoyan[33] , , W. Shaikh[109] , , A. Shangaraev[112] , , A. Sharma[98] , , A. Sharma[100] , , M. Sharma[100] , , M. Sharma[100] , , N. Sharma[98 ,127] , , A.I. Sheikh[137] , , K. Shigaki[45] , , Q. Shou[7] , , K. Shtejer[9 ,24] , , Y. Sibiriak[89] , , S. Siddhanta[53] , , K.M. Sielewicz[33] , , T. Siemiarczuk[85] , , S. Silaeva[89] , , D. Silvermyr[32] , , C. Silvestre[80] , , G. Simatovic[97] , , G. Simonetti[33] , , R. Singaraju[137] , , R. Singh[87] , , V. Singhal[137] , , T. Sinha[109] , , B. Sitar[36] , , M. Sitta[30] , , T.B. Skaali[19] , , M. Slupecki[125] , , N. Smirnov[141] , , R.J.M. Snellings[62] , , T.W. Snellman[125] , , J. Song[17] , , M. Song[142] , , F. Soramel[27] , , S. Sorensen[127] , , F. Sozzi[106] , , E. Spiriti[49] , , I. Sputowska[118] , , B.K. Srivastava[105] , , J. Stachel[103] , , I. Stan[67] , , P. Stankus[94] , , E. Stenlund[32] , , D. Stocco[114] , , M.M. Storetvedt[35] , , P. Strmen[36] , , A.A.P. Suaide[121] , , T. Sugitate[45] , , C. Suire[60] , , M. Suleymanov[14] , , M. Suljic[23] , , R. Sultanov[63] , , M. Šumbera[93] , , S. Sumowidagdo[48] , , K. Suzuki[113] , , S. Swain[66] , , A. Szabo[36] , , I. Szarka[36] , , U. Tabassam[14] , , J. Takahashi[122] , , G.J. Tambave[20] , , N. Tanaka[130] , , M. Tarhini[60] , , M. Tariq[15] , , M.G. Tarzila[86] , , A. Tauro[33] , , G. Tejeda Muñoz[2] , , A. Telesca[33] , , K. Terasaki[129] , , C. Terrevoli[27] , , B. Teyssier[132] , , D. Thakur[47] , , S. Thakur[137] , , D. Thomas[119] , , F. Thoresen[90] , , R. Tieulent[132] , , A. Tikhonov[61] , , A.R. Timmins[124] , , A. Toia[69] , , S.R. Torres[120] , , S. Tripathy[47] , , S. Trogolo[24] , , G. Trombetta[31] , , L. Tropp[38] , , V. Trubnikov[3] , , W.H. Trzaska[125] , , B.A. Trzeciak[62] , , T. Tsuji[129] , , A. Tumkin[108] , , R. Turrisi[55] , , T.S. Tveter[19] , , K. Ullaland[20] , , E.N. Umaka[124] , , A. Uras[132] , , G.L. Usai[22] , , A. Utrobicic[97] , , M. Vala[116 ,64] , , J. Van Der Maarel[62] , , J.W. Van Hoorne[33] , , M. van Leeuwen[62] , , T. Vanat[93] , , P. Vande Vyvre[33] , , D. Varga[140] , , A. Vargas[2] , , M. Vargyas[125] , , R. Varma[46] , , M. Vasileiou[84] , , A. Vasiliev[89] , , A. Vauthier[80] , , O. Vázquez Doce[104 ,34] , , V. Vechernin[136] , , A.M. Veen[62] , , A. Velure[20] , , E. Vercellin[24] , , S. Vergara Limón[2] , , R. Vernet[8] , , R. Vértesi[140] , , L. Vickovic[117] , , S. Vigolo[62] , , J. Viinikainen[125] , , Z. Vilakazi[128] , , O. Villalobos Baillie[110] , , A. Villatoro Tello[2] , , A. Vinogradov[89] , , L. Vinogradov[136] , , T. Virgili[28] , , V. Vislavicius[32] , , A. Vodopyanov[76] , , M.A. Völkl[103 ,102] , , K. Voloshin[63] , , S.A. Voloshin[139] , , G. Volpe[31] , , B. von Haller[33] , , I. Vorobyev[104 ,34] , , D. Voscek[116] , , D. Vranic[33 ,106] , , J. Vrláková[38] , , B. Wagner[20] , , H. Wang[62] , , M. Wang[7] , , D. Watanabe[130] , , Y. Watanabe[129 ,130] , , M. Weber[113] , , S.G. Weber[106] , , D.F. Weiser[103] , , S.C. Wenzel[33] , , J.P. Wessels[70] , , U. Westerhoff[70] , , A.M. Whitehead[99] , , J. Wiechula[69] , , J. Wikne[19] , , G. Wilk[85] , , J. Wilkinson[103 ,52] , , G.A. Willems[70] , , M.C.S. Williams[52] , , E. Willsher[110] , , B. Windelband[103] , , W.E. Witt[127] , , S. Yalcin[79] , , K. Yamakawa[45] , , P. Yang[7] , , S. Yano[45] , , Z. Yin[7] , , H. Yokoyama[130 ,80] , , I.-K. Yoo[17] , , J.H. Yoon[59] , , V. Yurchenko[3] , , V. Zaccolo[57] , , A. Zaman[14] , , C. Zampolli[33] , , H.J.C. Zanoli[121] , , N. Zardoshti[110] , , A. Zarochentsev[136] , , P. Závada[65] , , N. Zaviyalov[108] , , H. Zbroszczyk[138] , , M. Zhalov[95] , , H. Zhang[20 ,7] , , X. Zhang[7] , , Y. Zhang[7] , , C. Zhang[62] , , Z. Zhang[7 ,131] , , C. Zhao[19] , , N. Zhigareva[63] , , D. Zhou[7] , , Y. Zhou[90] , , Z. Zhou[20] , , H. Zhu[20] , , J. Zhu[7] , , A. Zichichi[25 ,11] , , A. Zimmermann[103] , , M.B. Zimmermann[33] , , G. Zinovjev[3] , , J. Zmeskal[113] , , S. Zou[7] ,

Affiliation notes

[i] Deceased
[ii] Dipartimento DET del Politecnico di Torino, Turin, Italy

[iii] Georgia State University, Atlanta, Georgia, United States
[iv] M.V. Lomonosov Moscow State University, D.V. Skobeltsyn Institute of Nuclear, Physics, Moscow, Russia
[v] Department of Applied Physics, Aligarh Muslim University, Aligarh, India
[vi] Institute of Theoretical Physics, University of Wroclaw, Poland

Collaboration Institutes

[1] A.I. Alikhanyan National Science Laboratory (Yerevan Physics Institute) Foundation, Yerevan, Armenia
[2] Benemérita Universidad Autónoma de Puebla, Puebla, Mexico
[3] Bogolyubov Institute for Theoretical Physics, Kiev, Ukraine
[4] Bose Institute, Department of Physics and Centre for Astroparticle Physics and Space Science (CAPSS), Kolkata, India
[5] Budker Institute for Nuclear Physics, Novosibirsk, Russia
[6] California Polytechnic State University, San Luis Obispo, California, United States
[7] Central China Normal University, Wuhan, China
[8] Centre de Calcul de l’IN2P3, Villeurbanne, Lyon, France
[9] Centro de Aplicaciones Tecnológicas y Desarrollo Nuclear (CEADEN), Havana, Cuba
[10] Centro de Investigación y de Estudios Avanzados (CINVESTAV), Mexico City and Mérida, Mexico
[11] Centro Fermi - Museo Storico della Fisica e Centro Studi e Ricerche “Enrico Fermi’, Rome, Italy
[12] Chicago State University, Chicago, Illinois, United States
[13] China Institute of Atomic Energy, Beijing, China
[14] COMSATS Institute of Information Technology (CIIT), Islamabad, Pakistan
[15] Department of Physics, Aligarh Muslim University, Aligarh, India
[16] Department of Physics, Ohio State University, Columbus, Ohio, United States
[17] Department of Physics, Pusan National University, Pusan, Republic of Korea
[18] Department of Physics, Sejong University, Seoul, Republic of Korea
[19] Department of Physics, University of Oslo, Oslo, Norway
[20] Department of Physics and Technology, University of Bergen, Bergen, Norway
[21] Dipartimento di Fisica dell’Università ’La Sapienza’ and Sezione INFN, Rome, Italy
[22] Dipartimento di Fisica dell’Università and Sezione INFN, Cagliari, Italy
[23] Dipartimento di Fisica dell’Università and Sezione INFN, Trieste, Italy
[24] Dipartimento di Fisica dell’Università and Sezione INFN, Turin, Italy
[25] Dipartimento di Fisica e Astronomia dell’Università and Sezione INFN, Bologna, Italy
[26] Dipartimento di Fisica e Astronomia dell’Università and Sezione INFN, Catania, Italy
[27] Dipartimento di Fisica e Astronomia dell’Università and Sezione INFN, Padova, Italy
[28] Dipartimento di Fisica ‘E.R. Caianiello’ dell’Università and Gruppo Collegato INFN, Salerno, Italy
[29] Dipartimento DISAT del Politecnico and Sezione INFN, Turin, Italy
[30] Dipartimento di Scienze e Innovazione Tecnologica dell’Università del Piemonte Orientale and INFN Sezione di Torino, Alessandria, Italy
[31] Dipartimento Interateneo di Fisica ‘M. Merlin’ and Sezione INFN, Bari, Italy
[32] Division of Experimental High Energy Physics, University of Lund, Lund, Sweden
[33] European Organization for Nuclear Research (CERN), Geneva, Switzerland
[34] Excellence Cluster Universe, Technische Universität München, Munich, Germany
[35] Faculty of Engineering, Bergen University College, Bergen, Norway
[36] Faculty of Mathematics, Physics and Informatics, Comenius University, Bratislava, Slovakia
[37] Faculty of Nuclear Sciences and Physical Engineering, Czech Technical University in Prague, Prague, Czech Republic
[38] Faculty of Science, P.J. Šafárik University, Košice, Slovakia
[39] Faculty of Technology, Buskerud and Vestfold University College, Tonsberg, Norway
[40] Frankfurt Institute for Advanced Studies, Johann Wolfgang Goethe-Universität Frankfurt, Frankfurt, Germany
[41] Gangneung-Wonju National University, Gangneung, Republic of Korea
[42] Gauhati University, Department of Physics, Guwahati, India
[43] Helmholtz-Institut für Strahlen- und Kernphysik, Rheinische Friedrich-Wilhelms-Universität Bonn, Bonn, Germany
[44] Helsinki Institute of Physics (HIP), Helsinki, Finland
[45] Hiroshima University, Hiroshima, Japan

[46] Indian Institute of Technology Bombay (IIT), Mumbai, India
[47] Indian Institute of Technology Indore, Indore, India
[48] Indonesian Institute of Sciences, Jakarta, Indonesia
[49] INFN, Laboratori Nazionali di Frascati, Frascati, Italy
[50] INFN, Laboratori Nazionali di Legnaro, Legnaro, Italy
[51] INFN, Sezione di Bari, Bari, Italy
[52] INFN, Sezione di Bologna, Bologna, Italy
[53] INFN, Sezione di Cagliari, Cagliari, Italy
[54] INFN, Sezione di Catania, Catania, Italy
[55] INFN, Sezione di Padova, Padova, Italy
[56] INFN, Sezione di Roma, Rome, Italy
[57] INFN, Sezione di Torino, Turin, Italy
[58] INFN, Sezione di Trieste, Trieste, Italy
[59] Inha University, Incheon, Republic of Korea
[60] Institut de Physique Nucléaire d'Orsay (IPNO), Université Paris-Sud, CNRS-IN2P3, Orsay, France
[61] Institute for Nuclear Research, Academy of Sciences, Moscow, Russia
[62] Institute for Subatomic Physics of Utrecht University, Utrecht, Netherlands
[63] Institute for Theoretical and Experimental Physics, Moscow, Russia
[64] Institute of Experimental Physics, Slovak Academy of Sciences, Košice, Slovakia
[65] Institute of Physics, Academy of Sciences of the Czech Republic, Prague, Czech Republic
[66] Institute of Physics, Bhubaneswar, India
[67] Institute of Space Science (ISS), Bucharest, Romania
[68] Institut für Informatik, Johann Wolfgang Goethe-Universität Frankfurt, Frankfurt, Germany
[69] Institut für Kernphysik, Johann Wolfgang Goethe-Universität Frankfurt, Frankfurt, Germany
[70] Institut für Kernphysik, Westfälische Wilhelms-Universität Münster, Münster, Germany
[71] Instituto de Ciencias Nucleares, Universidad Nacional Autónoma de México, Mexico City, Mexico
[72] Instituto de Física, Universidade Federal do Rio Grande do Sul (UFRGS), Porto Alegre, Brazil
[73] Instituto de Física, Universidad Nacional Autónoma de México, Mexico City, Mexico
[74] IRFU, CEA, Université Paris-Saclay, Saclay, France
[75] iThemba LABS, National Research Foundation, Somerset West, South Africa
[76] Joint Institute for Nuclear Research (JINR), Dubna, Russia
[77] Konkuk University, Seoul, Republic of Korea
[78] Korea Institute of Science and Technology Information, Daejeon, Republic of Korea
[79] KTO Karatay University, Konya, Turkey
[80] Laboratoire de Physique Subatomique et de Cosmologie, Université Grenoble-Alpes, CNRS-IN2P3, Grenoble, France
[81] Lawrence Berkeley National Laboratory, Berkeley, California, United States
[82] Moscow Engineering Physics Institute, Moscow, Russia
[83] Nagasaki Institute of Applied Science, Nagasaki, Japan
[84] National and Kapodistrian University of Athens, Physics Department, Athens, Greece
[85] National Centre for Nuclear Studies, Warsaw, Poland
[86] National Institute for Physics and Nuclear Engineering, Bucharest, Romania
[87] National Institute of Science Education and Research, HBNI, Jatni, India
[88] National Nuclear Research Center, Baku, Azerbaijan
[89] National Research Centre Kurchatov Institute, Moscow, Russia
[90] Niels Bohr Institute, University of Copenhagen, Copenhagen, Denmark
[91] Nikhef, Nationaal instituut voor subatomaire fysica, Amsterdam, Netherlands
[92] Nuclear Physics Group, STFC Daresbury Laboratory, Daresbury, United Kingdom
[93] Nuclear Physics Institute, Academy of Sciences of the Czech Republic, Řež u Prahy, Czech Republic
[94] Oak Ridge National Laboratory, Oak Ridge, Tennessee, United States
[95] Petersburg Nuclear Physics Institute, Gatchina, Russia
[96] Physics Department, Creighton University, Omaha, Nebraska, United States
[97] Physics department, Faculty of science, University of Zagreb, Zagreb, Croatia
[98] Physics Department, Panjab University, Chandigarh, India
[99] Physics Department, University of Cape Town, Cape Town, South Africa
[100] Physics Department, University of Jammu, Jammu, India

[101] Physics Department, University of Rajasthan, Jaipur, India
[102] Physikalisches Institut, Eberhard Karls Universität Tübingen, Tübingen, Germany
[103] Physikalisches Institut, Ruprecht-Karls-Universität Heidelberg, Heidelberg, Germany
[104] Physik Department, Technische Universität München, Munich, Germany
[105] Purdue University, West Lafayette, Indiana, United States
[106] Research Division and ExtreMe Matter Institute EMMI, GSI Helmholtzzentrum für Schwerionenforschung GmbH, Darmstadt, Germany
[107] Rudjer Bošković Institute, Zagreb, Croatia
[108] Russian Federal Nuclear Center (VNIIEF), Sarov, Russia
[109] Saha Institute of Nuclear Physics, Kolkata, India
[110] School of Physics and Astronomy, University of Birmingham, Birmingham, United Kingdom
[111] Sección Física, Departamento de Ciencias, Pontificia Universidad Católica del Perú, Lima, Peru
[112] SSC IHEP of NRC Kurchatov institute, Protvino, Russia
[113] Stefan Meyer Institut für Subatomare Physik (SMI), Vienna, Austria
[114] SUBATECH, IMT Atlantique, Université de Nantes, CNRS-IN2P3, Nantes, France
[115] Suranaree University of Technology, Nakhon Ratchasima, Thailand
[116] Technical University of Košice, Košice, Slovakia
[117] Technical University of Split FESB, Split, Croatia
[118] The Henryk Niewodniczanski Institute of Nuclear Physics, Polish Academy of Sciences, Cracow, Poland
[119] The University of Texas at Austin, Physics Department, Austin, Texas, United States
[120] Universidad Autónoma de Sinaloa, Culiacán, Mexico
[121] Universidade de São Paulo (USP), São Paulo, Brazil
[122] Universidade Estadual de Campinas (UNICAMP), Campinas, Brazil
[123] Universidade Federal do ABC, Santo Andre, Brazil
[124] University of Houston, Houston, Texas, United States
[125] University of Jyväskylä, Jyväskylä, Finland
[126] University of Liverpool, Liverpool, United Kingdom
[127] University of Tennessee, Knoxville, Tennessee, United States
[128] University of the Witwatersrand, Johannesburg, South Africa
[129] University of Tokyo, Tokyo, Japan
[130] University of Tsukuba, Tsukuba, Japan
[131] Université Clermont Auvergne, CNRS/IN2P3, LPC, Clermont-Ferrand, France
[132] Université de Lyon, Université Lyon 1, CNRS/IN2P3, IPN-Lyon, Villeurbanne, Lyon, France
[133] Université de Strasbourg, CNRS, IPHC UMR 7178, F-67000 Strasbourg, France, Strasbourg, France
[134] Università degli Studi di Pavia, Pavia, Italy
[135] Università di Brescia, Brescia, Italy
[136] V. Fock Institute for Physics, St. Petersburg State University, St. Petersburg, Russia
[137] Variable Energy Cyclotron Centre, Kolkata, India
[138] Warsaw University of Technology, Warsaw, Poland
[139] Wayne State University, Detroit, Michigan, United States
[140] Wigner Research Centre for Physics, Hungarian Academy of Sciences, Budapest, Hungary
[141] Yale University, New Haven, Connecticut, United States
[142] Yonsei University, Seoul, Republic of Korea
[143] Zentrum für Technologietransfer und Telekommunikation (ZTT), Fachhochschule Worms, Worms, Germany